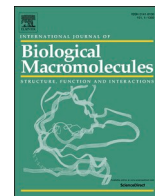




Since January 2020 Elsevier has created a COVID-19 resource centre with free information in English and Mandarin on the novel coronavirus COVID-19. The COVID-19 resource centre is hosted on Elsevier Connect, the company's public news and information website.

Elsevier hereby grants permission to make all its COVID-19-related research that is available on the COVID-19 resource centre - including this research content - immediately available in PubMed Central and other publicly funded repositories, such as the WHO COVID database with rights for unrestricted research re-use and analyses in any form or by any means with acknowledgement of the original source. These permissions are granted for free by Elsevier for as long as the COVID-19 resource centre remains active.



# Chitosan derivatives: A suggestive evaluation for novel inhibitor discovery against wild type and variants of SARS-CoV-2 virus

Chandrima Modak<sup>a,1</sup>, Anubhuti Jha<sup>b,1</sup>, Nivya Sharma<sup>c</sup>, Awanish Kumar<sup>b,\*</sup>

<sup>a</sup> Birla Institute of Technology and Sciences (BITS), Pilani campus, Rajasthan, India

<sup>b</sup> Department of Biotechnology, National Institute of Technology (NIT), Raipur, Chhattisgarh, India

<sup>c</sup> Department of Pharmacology & Toxicology, National Institute of Pharmaceutical Education and Research (NIPER), Hyderabad, Telangana, India

## ARTICLE INFO

### Keywords:

Chitosan  
Derivatives  
Marine carbohydrate  
SARS-CoV-2 variants  
Spike protein  
Anti-COVID-19 therapeutics

## ABSTRACT

With increasing global cases and mortality rates due to COVID-19 infection, finding effective therapeutic interventions has become a top priority. Marine resources are not explored much and to be taken into consideration for exploring antiviral potential. Chitosan (carbohydrate polymer) is one such bioactive glycan found ubiquitously in marine organisms. The presence of reactive amine/hydroxyl groups, with low toxicity/allergenicity, compels us to explore it against SARS-CoV-2. We have screened a library of chitosan derivatives by site-specific docking at not only spike protein Receptor Binding Domain (RBD) of wild type SARS-CoV-2 but also on RBD of B.1.1.7 (UK) and P.1 (Brazil) SARS-CoV-2 variants. The obtained result was very interesting and ranks N-benzyl-O-acetyl-chitosan, Imino-chitosan, Sulfated-chitosan oligosaccharides derivatives as a potent antiviral candidate due to its high binding affinity of the ligands (-6.0 to -6.6 kcal/mol) with SARS-CoV-2 spike protein RBD and they critically interacting with amino acid residues Tyr 449, Asn 501, Tyr 501, Gln 493, Gln 498 and some other site-specific residues associated with higher transmissibility and severe infection. Further ADMET analysis was done and found significant for exploration of the future therapeutic potential of these three ligands. The obtained results are highly encouraging in support for consideration and exploration in further clinical studies of these chitosan derivatives as anti-SARS-CoV-2 therapeutics.

## 1. Introduction

COVID-19 infection was reported as an unknown pneumonia-like infection for the first time, in Wuhan, China towards the end of the year 2019. Later it was determined to be caused by SARS-CoV-2 virus, a beta-coronavirus closely related to the other CoVs such as SARS and Bat coronavirus RaTG13 [1] in lineage B subtype of beta coronaviruses belonging to the *Coronavirinae* subfamily, covered under the broad umbrella of the *Coronaviridae* family [2]. The infection, mortality, and morbidity rate of the virus were significantly high. With COVID-19 infection inflicting harm around the world, finding effective therapeutic interventions became a top priority and is sustained to be with the emergence of mutant variants of the virus. Global efforts to develop highly efficient and safe vaccines to combat COVID-19 infection causing virus have met with varying degrees of success in terms of vaccine design but the emergence of SARS-CoV-2 variants [B.1.1.7 (UK) and P.1 (Brazil)] is markedly more resistant to neutralization by vaccine [3].

These variants with similar spike mutations present new challenges for prophylaxis and threaten the protective efficacy of current vaccines. Therefore it is an urgent need to discover some therapeutics to combat effectively with wild-type strain as well as variants of SARS-CoV-2. A significant number of antiviral drugs have been in clinical trials for the treatment of hospitalized and critically ill patients in the last year. However, the majority of them have been ineffective against SARS-CoV-2 pathogenesis. New data suggest the various infection-causing pathways and the receptors and enzymes involved as drug targets sites that can be exploited for stopping the infection cycle of the SARS-CoV-2 virus. One of the notable targets has been the Spike protein, a glycoprotein on the virus surface which is pivotal for its binding to a wide variety of host cell receptors (Fig. 1). Also, greater concern has been associated with this glycoprotein due to its fast pace mutation, and its effects on the efficacy of existing therapeutics. Notably, advances in vaccine development have been a global initiative [4]. Moreover, the spontaneous mutation from wild-type variants caused by secondary

\* Corresponding author at: Department of Biotechnology, National Institute of Technology, Raipur 492010, CG, India.

E-mail address: [awanik.bt@nitrr.ac.in](mailto:awanik.bt@nitrr.ac.in) (A. Kumar).

<sup>1</sup> Equal first authorship.

<https://doi.org/10.1016/j.ijbiomac.2021.07.144>

Received 15 April 2021; Received in revised form 14 July 2021; Accepted 20 July 2021

Available online 27 July 2021

0141-8130/© 2021 Elsevier B.V. All rights reserved.

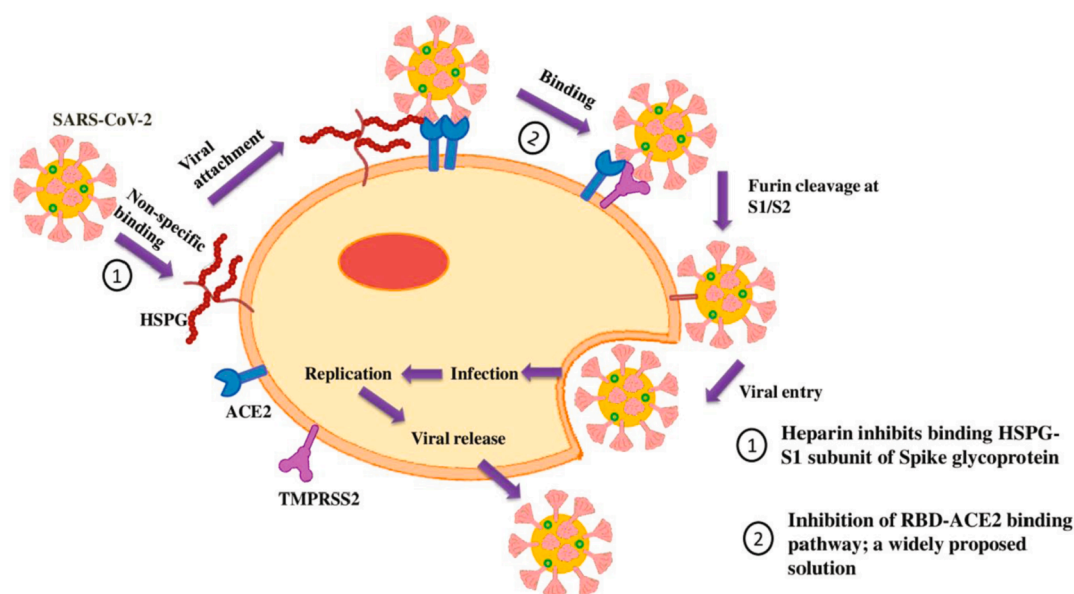


Fig. 1. Mechanism of viral attachment and viral entry. Potential drug targets in viral infection pathway.

transmission has brought out greater concerns of intolerance to therapeutic interventions. This calls for rational designing of efficacious treatment strategies to robustly tackle this pandemic by targeting various pathways and mechanisms of infection by either creating new drug molecules or repurpose already existing drug molecules for impacting virus infection cycle or structural proteins [2].

The molecules derived from marine resources are no less in this consideration as potent antivirals. One such primarily marine-resourced bioactive macromolecule is Chitosan. Although much attention has been not covered with respect to marine resources as potential drug therapeutic molecules, recent reports of chitosan as a plausible molecule for fighting COVID-19 disease are well documented in review literature by Sharma et al. [5]. Chitosan is chitin (second to cellulose in terms of wide availability as a polysaccharide) derivative and is structural, a randomly deacetylated copolymer of  $\beta$ -(1-4)-linked d-glucosamine and N-acetyl-d-glucosamine [6]. In the past few decades, Chitosan has been well explored as a potent antimicrobial, alone or in combination with other compounds [7]. It is also well acknowledged as an antiviral agent in an extensive review by Chirkov [8]. A quaternized chitosan derivative, N-(2-hydroxypropyl)-3-trimethylammonium chitosan chloride (HTCC) has been notable in impeding the growth of a wide range of human coronaviruses, inhibition varying with different substitutions [9].

The SARS-CoV-2 virus has four different proteins, crucial for running its infection cycle and replication process. These proteins are spike glycoprotein, small envelope glycoprotein, membrane glycoprotein, and nucleocapsid protein, each playing a well-defined role [10]. Of all these, spike protein has been looked upon as a major target responsible for infection initiation. It is a homotrimeric peptide with each monomer having two distinct, S1 and S2 subunits. S1 subunit is dissociated upon binding of spike protein with Angiotensin-Converting Enzyme 2 (ACE2) receptors which stimulate the S2 subunit to come into a stable state required for membrane fusion for facilitating virus entry into the host cell [11]. Spike protein has been reported to acquire two different forms, an unstable pre-fusion (closed state) and a stable post-fusion (open state). The latter state entails exposed Receptor binding domain which has specificity towards ACE2 receptors, opposite to the former one [12]. While the interaction of spike protein with human ACE2 receptors has gained significant attention [13], binding of RBD of S1 subunit of spike protein to heparan sulfate site, a site adjacent to ACE2 receptor site has recently been talked about. This latter type of binding has been shown to enhance the interactions between ACE2 and spike protein of the virus by

favouring RBD open conformation [14].

This paper does the computational screening of a library of already reported antimicrobial and/or antiviral chitosan derivatives for evaluating their activities towards the pre-fusion and post-fusion states of the spike protein. As aforementioned, the pre-fusion state favors binding to the heparan sulfate site and the postfusion state is pivotal for binding to ACE2 receptors to assist virus access inside the host cell. Heparin disaccharide was taken as a positive control for the former interaction and ACE2 receptor as a positive control for the latter one. This exercise led to the identification of three chitosan derivatives, namely N-benzyl-O-acetyl-chitosan, Imino-chitosan, and Sulfated-chitosan oligosaccharides with relatively higher binding affinities and site-specificity. N-benzoyl-O-acetyl-chitosan is prepared from chitosan after partial acylation. This is a novel derivative in the sense that it has not been studied for its antiviral activity to date. However, its reported antibacterial and antifungal activities reflect superior action compared to chitosan alone. The protonation of amino groups, high hydrophobicity, and presence of benzyl group (antimicrobial and antifungal) was proposed as plausible mechanisms behind enhanced penetration of this compound into the microbial cell membranes [15]. A variety of Imino-chitosan biopolymeric films synthesized by acid condensation of amino groups of chitosan with different aldehydes have shown strong antimicrobial properties, compared to chitosan control [16]. Conversely, sulfated-chitosan oligosaccharide has been reported to show activity against HIV-1 infection [17]. None of these molecules have been explored against SARS-CoV-2 virus targets and thus, making this study novel.

With support from computational data, this paper presents the rationale selection of the top three chitosan derivatives with superior anti-SARS-CoV-2 activity from the library of screened antiviral chitosan derivatives. Studies undertaken were the blind and active site-specific docking studies amalgamated with the homology modeling, performed to evaluate the potential of top three selected derivatives against other coronavirus strains, harboring similarity in the structural proteins to some extent. The top-performing ligands have also been docked against the mutated variants of the SARS-CoV-2 virus, namely Brazilian and UK strains to validate their binding consistency. To understand the activity of the selected derivatives against other virus targets, they were docked against the virus main protease enzyme, taking Boceprevir as the positive control. ADMET analysis of the three selected derivatives was done to evaluate their pharmacokinetic potential for future clinical usage. This paper puts due focus on the antiviral worth of marine resources and

**Table 1**Interaction overview of Chain E (RBD) and Chain A (ACE2); PDB ID 6M0J at  $\leq 3.5$  Å.

Interaction overview at (3.5 Å)	
Number of interacting residues Chain E	14
Number of interacting residues Chain A	15
Number of hydrophilic-hydrophobic interaction	5
Number of hydrophilic-hydrophilic interaction	15
Number of hydrophobic-hydrophobic interaction	1

very strongly supports the further pharmacological evaluations of the top three performers.

## 2. Materials and methods

### 2.1. Molecular docking for protein-ligand interaction

UCSF Chimera 1.15r was used for receptors and ligand preparation (<https://www.cgl.ucsf.edu/chimera/>). They were written in mol2 format (20), and for the generation of executable format for AutodockVina, Autodock tools 4.2 was used with all the conformation properties reserved as in mol2 format, for binding analysis Autodockvina 1.1.2 site package (latest version, updated 2011) was used (21). The ligand-receptor visualization was done using BIOVIA Discovery Studio (Design LI. Pharmacophore and ligand-based design with Biovia Discovery Studio®).

#### 2.1.1. Target selection

Due to lack of effective drugs targeting inhibition of the interaction between Angiotensin-converting enzyme 2 receptor (ACE2)-spike glycoprotein, a library of ACE2 binding residues of the receptor-binding domain (RBD) exposed open conformation of S1 subunit of S-glycoprotein were selected as target site (13). Furthermore, the putative heparin/heparan sulfate binding residues were selected as a target site for closed conformation of S-glycoprotein (16).

#### 2.1.2. Ligand preparations

Two sets of properties were considered for protein-ligand docking, i. e., Chitosan native and Chitosan derivatives that had shown activity as antiviral and/or antimicrobial. The three-dimensional molecular structure of these chitosan derivatives was retrieved from the PubChem database. Some derivatives were not considered for further docking which was reported as antiviral and/or antimicrobial. This is due to the scoring function limitations of AutodockVina of up to 20 flexible bonds (22), along with the problem that they can't be broken down to smaller monomers, or dimers as they lose the structural properties. UCSF chimera tools were used in structure generation from the PubChem database, and energy minimization for each ligand, done individually with conjugate descent steps of 100 was taken with a step size of 0.02 Angstroms and along with default parameters such as steepest descent steps of 100 with a step size of 0.02 Angstroms, and update interval of 10. Finally, Dock prep of each model of each ligand was done by the addition of gasteiger charges (23), and hydrogens were written in .mol2 format and later converted to Autodockvina executable format with the help of Autodock tools.

#### 2.1.3. Receptor preparation

Docking of the prospective molecules was done at ACE2 bound site of RBD of S-glycoprotein PDB ID: 6M0J with a low resolution of 2.45 Å [11] was used to target the ACE2 binding residues of the RBD of SARS-CoV-2 as the active target site. For heparan sulfate proteoglycan/heparin-binding site as target site, the homotrimerectodomain in pre-fusion state of S-glycoprotein PDB ID: 6X79 with a low resolution of 2.90 Å was considered [18]. For comparative studies on the impact of changes in residues for variants UK B1.1.7 lineage and Brazil variant P.1

Lineage, PDB IDs 7NEG and 7NXC were taken respectively [19,20]. For the main protease the PDB ID: 7BRO with a low resolution of 2.00 Å was considered [21]. All the protein x-ray crystallographic structures were accessed from the RCSB protein data bank. Before docking of ligand and receptor docking, the stereochemical quality of the respective protein structures was determined by the PROCHECK SUITE program [22]. Dock prep was done for each receptor water, and all non-standard residues were ignored, missing residues, gasteiger charges, polar hydrogens were added as per default parameters [23] of chimera and were saved in Autodockvina executable format.

### 2.2. Protein-protein interaction

To determine the residues interaction and buried surface between Receptor Binding Domain (RBD) and ACE2 complex CoCoMAPS tools were used at RMSF ( $\leq 3.5$  Å i.e., Å) [24–26], as higher distance causes weak hydrogen bonds. The flexibility of the RBD (Chain E of PDB ID: 6M0J and 7NXC) was determined by the CABS flex site package [27,28].

### 2.3. Screen and selection of ligands

A selected library of chitosan and chitosan derivatives with antimicrobial/antiviral properties available in the Pubchem database were roughly screened with Pyrx tools with a more extensive search volume, i. e.,  $>30 \times 30 \times 30$ . Out of them, binding affinity higher than -6.0 kcal/mol were further docked within search volume of  $25 \times 25 \times 25$ , the grid parameters for the model used are 6M0J (for center\_XYZ -38.27, 25.64, 4.40), 7NEG (for center\_XYZ-44.34, 11.74, 12.05), 7NXC (for center\_XYZ-36.29, 26.41, 7.12). For  $6 \times 79$  (for center\_XYZ200.76, 178.16, 160.31 and search volume  $20 \times 20 \times 20$ ), and 7BRO (for center\_XYZ 11.83, -14.38, 20.14 and search volume  $18 \times 18 \times 18$ ) with exhaustiveness of 100 for all. There was a significant reduction in binding affinity in further docking, and out of them, the least explored novel derivatives such as N-benzyl-O-acetyl-chitosan, Imino-chitosan were further docked, and anti-HIV derivative Sulfated-chitosan oligosaccharide was also explored.

### 2.4. Bioactivity prediction

The bioactivity and physicochemical properties of three test ligand derivatives as a potent drug lead were carried out by Molinspiration (<http://www.molinspiration.com/cgi-bin/properties>) (32). The bioactivity score consists of several physicochemical properties like Molecular weight & Volume, LogP, Molecular polar surface area (PSA) details of the number of atoms (n-atoms), and Rotatable Bonds (nrotb). Based on these properties, this software analyses the fitness of a ligand-based on its chemical structure.

### 2.5. ADMET prediction

ADMET properties of a compound deal with its absorption, distribution, metabolism, excretion, and toxicity in and through the human body. ADMET, which constitutes the pharmacokinetic profile of a drug molecule, is very essential in evaluating its pharmacodynamic activities. Today a lot of online tools and offline software programs are available which help us in predicting the behaviour of the drug candidate. In this study, we have used the <http://admet.scbdd.com/calcprehttps://preadmet.bmdrc.kr/adme/> and admetSAR prediction tool (<http://lmmdd.ecust.edu.cn:8000/>) (33).

## 3. Results and discussion

### 3.1. ACE2 receptor and SARS-CoV-2 RBD interaction

ACE2 receptor has been reported as the primary specific target receptor for SARS-CoV-2 viral entry [29]. An array of 14 amino acid

**Table 2**

Accessibility surface area (ASA) between Chain E (RBD) and Chain A(ACE2); PDB ID 6MOJ at  $\leq 3.5$  Å.

Buried area upon the complex formation (Å) <sup>2</sup>	1688.8
Buried area upon the complex formation (%)	4.72
Interface area (Å) <sup>2</sup>	844.4
Interface area Chain E (%)	8.36
Interface area Chain A (%)	3.29
POLAR Buried area upon the complex formation (Å) <sup>2</sup>	974.1
POLAR Buried area upon the complex formation (%)	57.68
POLAR Interface area (Å) <sup>2</sup>	487.05
NO POLAR Buried area upon the complex formation ((Å) <sup>2</sup> <sup>2</sup> / sup>)	714.7
NO POLAR Buried area upon the complex formation (%)	42.32
NO POLAR Interface area (Å) <sup>2</sup>	357.35
Residues at the interface.TOT (n)	49
Residues at the interface.Chain E (n)	24
Residues at the interface.Chain A (n)	25

residues of RBD of SARS-CoV-2 (wild type) binds to ACE2 at RMSF ( $\leq 3.5$  Å) summarized in Tables 1, 2, and Fig. 2, along with the disulfide bonds. These residues play a significant role in higher binding affinity

and stable binding of the spike glycoprotein of SARS-CoV-2 to ACE2 receptor in comparison to other beta coronaviruses of the same lineage specifically SARS-CoV. Viruses sharing a similar phenotype that of SARS-CoV-2 cause severe respiratory infection in humans. To summarize, the key features that make ACE2 susceptible to RBD of SARS-CoV-2 are a) presence of 9 cysteines out of which 8 of cysteine for four pairs of disulfide bonds out of which three (Cys336–Cys361 (2), Cys379–Cys432, and Cys391–Cys525) [11,12,30,31] provide stability to beta-sheets and one (Cys480–Cys488) [31] that connects the loop in the distal end of Receptor Binding Motif (RBM). b) participation of virus binding hotspots residues Lys 31 and Lys 353 of N-terminal peptidase of ACE2 (Fig. 3) that was previously reported to be pivotal for binding to SARS-CoV-2 RBM due to the charge neutralization by lysine [32,33]. Moreover, this characteristic of these residues of ACE2 is well reserved in case of binding to SARS-CoV-2. Initially, a hydrogen bond is formed between Lys 31 (ACE2) and Gln 493 (RBD) but experiences low stability due to the bulky side chain's absences around Leu 455 residue leading to breaking off the bond between Gln 493 (RBD) and Lys 31 (ACE2) with the formation of a stronger hydrogen bond between Gln 493 (RBD) and Glu 35 (ACE2) [12,34], and Lys 31 (ACE2) forming an attractive

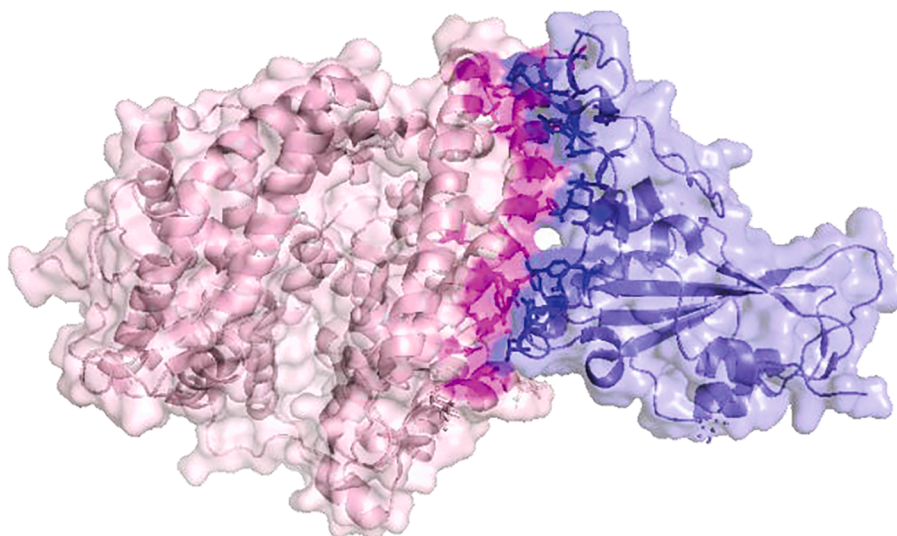


**Fig. 2.** Residues interaction between RBD of SARS-CoV-2 and ACE-2 N-terminal peptidase at RMSF ( $\leq 3.5$  Å).

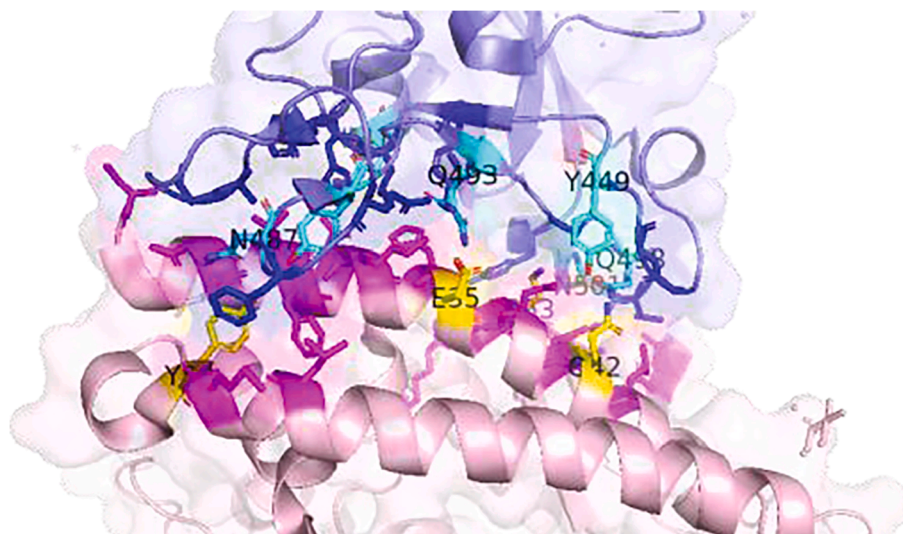


**Fig. 3.** Essential residues of RBD of SARS-CoV-2 and ACE2 that make SARS-CoV-2 more virulent than SARS-CoV.

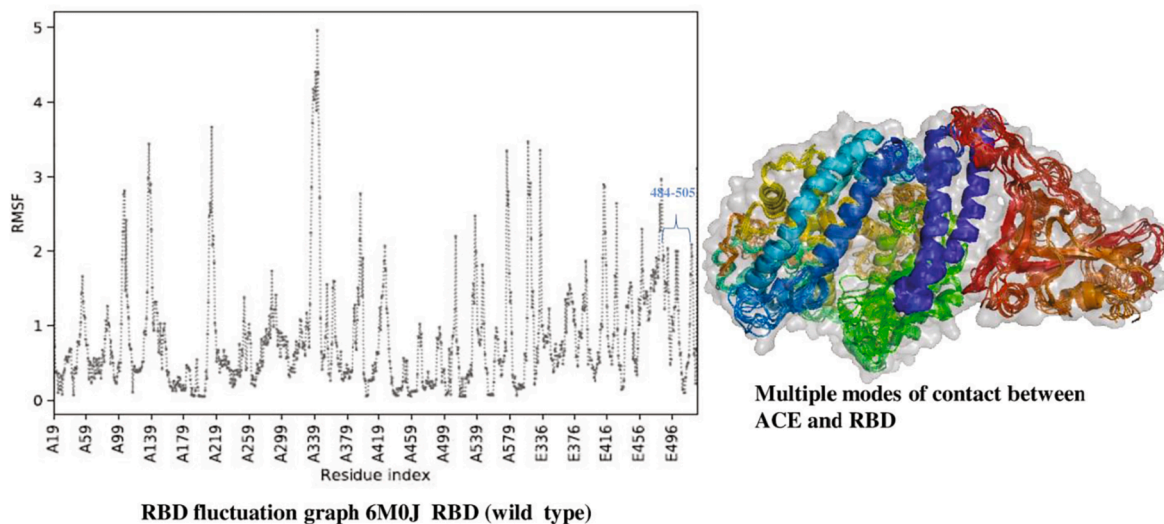


Fig. 4. Comparison of the configuration of RBD of wild type with new mutated variants B.1.1.7 and P.1 lineage.

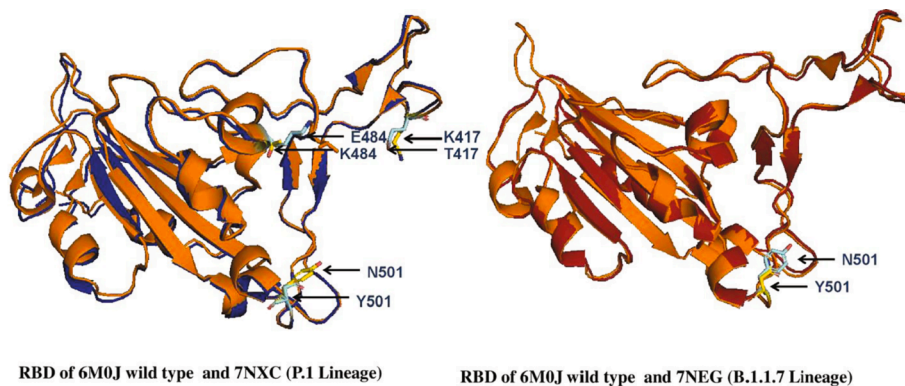


Fig. 5. Contact Simulation and Fluctuation of Chain E of 6M0J (RBD) protein with Chain A 6M0J (ACE2).

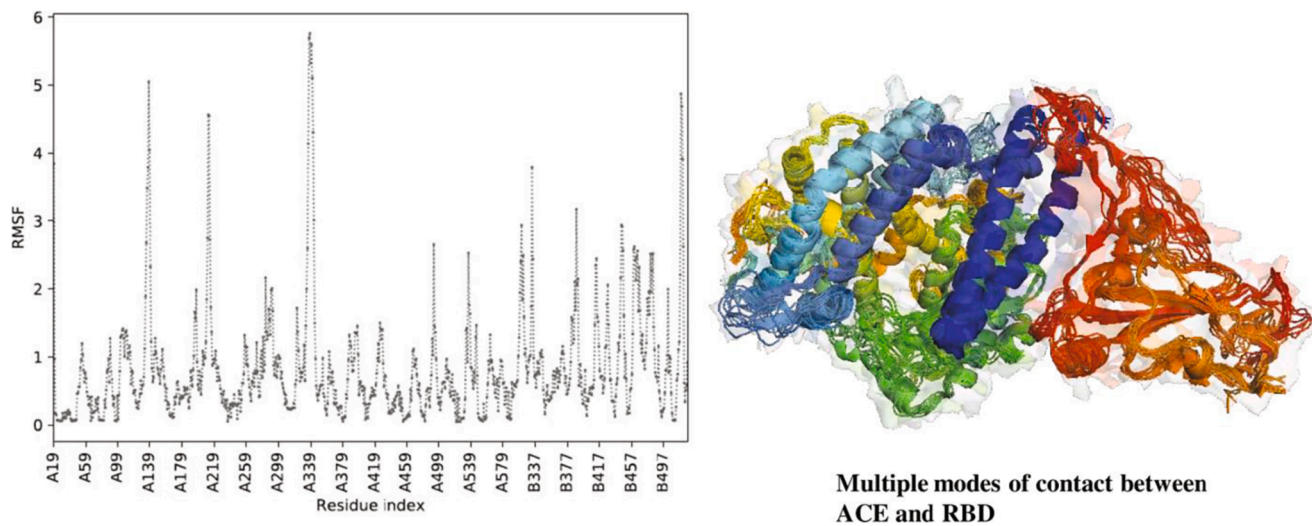


Fig. 6. Contact Simulation and Fluctuation of Chain B of 7NXC (RBD) protein with Chain A 7NXC (ACE2).

**Table 3**Comparison of the residue of RBD and ACE2; PDB ID 7NXC P.1 a lineage (Brazil variant) and PDB ID 6M0J wild type at  $\leq 3.5$  Å.

Interaction overview at $\leq 3.5$ Å				
Chemical bonds	SARS-CoV-2 P.1 lineage		SARS-CoV-2 wild-type	
	Residues	Length (Å)	Residues	Length (Å)
Hydrogen bonds	TYR 449 (OH)	2.99	ASN487 (ND2)	2.6
	TYR 501 (CE1)	3.3	LYS417 (NZ)	3.0
	TYR 505 (CD2)	3.37	GLN493 (NE2)	2.8
	THR 500 (OG1)	2.45	TYR505 (OH)	3.2
	ASN 487 (ND2)	2.42	TYR449 (OH)	2.7
	GLN 498 (OE1)	3.45	THR500 (OG1)	2.6
	GLN 493 (NE2)	3.1	ASN501 (N)	3.7
	ASN 487 (OD1)	2.77	TYR449 (OH)	3.0
	TYR 501 (OH)	3.32	TYR489 (OH)	3.5
	THR 500 (CB)	3.45	ASN487 (OD1)	2.7
	TYR 453 (OH)	3.17	GLY 502 (N)	2.8
	TYR 489 (OH)	3.41	TYR505 (OH)	3.7
	GLN 498 (OE1)	3.1	GLN 498 (OE1)*	3.58
	Other bonds			LYS417 (NZ) <sup>a</sup>
			LYS417 (NZ) <sup>a</sup>	3.0

<sup>a</sup> Salt bridge, HH: hydrogen eta, OD1: oxygen delta 1, OG1: oxygen gamma 1, O: oxygen, HN: nitrogen eta, NZ: nitrogen zeta, CD: carbon delta, CA: carbon alpha, HH11: hydrogen eta 11, HH12: hydrogen eta 12, HE22: hydrogen epsilon 22, HG1: hydrogen gamma 1, OE1: oxygen epsilon 1, ND2: nitrogen delta 2, NE2: nitrogen epsilon 2, OH: oxygen eta, N: nitrogen.

\* To highlight the presence of a higher bond length ( $\leq 3.5$  Å.) between two interacting proteins.

**Table 4**Interaction overview of Chain B (RBD) and Chain A (ACE2); PDB ID 7NXC a P.1 Lineage (Brazil variant) at  $\leq 3.5$  Å.

Interaction overview at $\leq 3.5$ Å	
Number of interacting residues Chain A	12
Number of interacting residues Chain B	12
Number of hydrophilic-hydrophobic interaction	4
Number of hydrophilic-hydrophilic interaction	13
Number of hydrophobic-hydrophobic interaction	1

**Table 5**Accessibility surface area (ASA) between Chain B (RBD) and Chain A (ACE2); PDB ID 7NXC a P.1 lineage (Brazil variant) at  $\leq 3.5$  Å.

Buried area upon the complex formation (Å) <sup>2</sup>	1729.6
Buried area upon the complex formation (%)	4.8
Interface area (Å) <sup>2</sup>	864.8
Interface area Chain A (%)	3.36
Interface area Chain B (%)	8.37
POLAR Buried area upon the complex formation (Å) <sup>2</sup>	1001.4
POLAR Buried area upon the complex formation (%)	57.9
POLAR Interface area (Å) <sup>2</sup>	500.7
NO POLAR Buried area upon the complex formation ((Å) <sup>2</sup> <sup>2</sup></sup>	728.2
NO POLAR Buried area upon the complex formation (%)	42.1
NO POLAR Interface area (Å) <sup>2</sup>	364.1
Residues at the interface_TOT (n)	48
Residues at the interface_Chain A (n)	24
Residues at the interface_Chain B (n)	24

electrostatic bond with Glu 484. Lys 353 (ACE2) seen to form a hydrogen bond with Gln 496 and Tyr 502, Tyr 505. However, according to Ali and Vijayan's Molecular dynamics simulations, Lys 353 of ACE2 forms hydrogen with Gln 498 of SARS-CoV-2 [34] contributing to the binding affinity between SARS-CoV-2-RBD and ACE2 (Fig. 3). The contacts formed between hotspots residues Lys 31 and Lys 353 of ACE2 provide low fluctuation in loop Tyr 484-Tyr 505 of RBD of SARS-CoV-2 determined using CABS flex 2.0 package. This observation (Fig. 4) is in agreement with the Molecular dynamics simulations done by Ali and Vijayan [34]. c) Stable hydrogen bond between Tyr 449 of RBD and Asp 38 of ACE2 has been another significant contributor to the virulence of

the SARS-CoV-2 virus [34]. Also, this hydrogen bond is aided by a hydrogen bond formed between Tyr 449 of RBD and Gln 42 of ACE2. d) Lastly the outer salt bridge formed by Lys 417 of SARS-CoV-2 has been one of the striking feature contributing to its higher binding affinity to ACE2 receptor (Fig. 3) [11,34,35]. This salt bridge was supported by an attractive charge between the hotspot residue Lys 31 and Glu 484.

Furthermore, recent developments of highly contagious new variants such as the B.1.1.7, B.1.351, and P.1 lineage have surfaced with new concerns. In December of 2020, Chand et al. submitted the first report of sequence detection of the B.1.1.7 variant, which contributes to the latest rise in cases by 40-80% and became one of the dominant variants [36,37], although several other mutations have occurred in the overall spike glycoprotein. However, the marked change that is standard for all three types is the mutation of residue Asn 501 to Tyr 501 on RBD of SARS-CoV-2 [38] (Fig. 5). Mutation of residue Glu 484 to Lys 484 has advanced the opportunity to escape neutralizing antibodies for the Spike protein [39]. A study reported by Supasa et.al suggested mutation of residue Asn 501 to Tyr 501 in B.1.1.7 variant has raised the binding affinity of ACE2 to RBD; it has also contributed to dodging the neutralizing monoclonal antibodies (mAbs), potentially jeopardizing the efficacy of current vaccines [19]. On mapping interaction of P.1 Lineage variant of SARS-CoV-2 RBD with ACE2 at RMSF ( $\leq 3.5$  Å), it was observed that there was a significantly lower fluctuation in loop 484-509 (Fig. 6) compared to that of the previous wild type strain; this observation can be attributed to the mutation of Glu 484 to Lys 484, Lys 417 to Thr 417 and Asn 501 to Tyr 501. The striking feature of the salt bridge formed by Lys 417 is absent in the case of a mutated variant. Also, there are direct interactions observed between the hotspots residues Glu 35, Asp 38, Tyr 41, Gln 42, Lys 353 (ACE2) and residues Gln 493, Tyr 449, Gln 498, and Tyr 501 of RBD along with most of the other interaction previously seen with the wild type Table 3. This contributed to lowering of fluctuation in the ACE2 burial region of RBD with an increase in the overall burial area of ACE2 (Tables 4-5). It is to be noted that these residues' mutations did not contribute to any significant geometric change of RBD (Fig. 5). These indicate the confidence in the residue selection for ACE2 binding sites as the active target site for identifying potential molecules inhibiting SARS-CoV-2 RBD binding to ACE2 for RBD exposed open conformation state.

**Table 6**

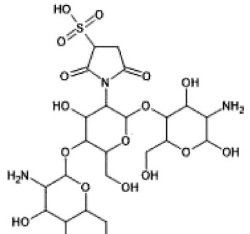
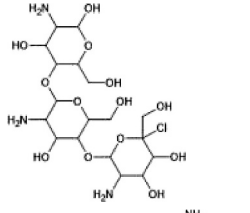
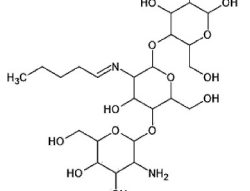
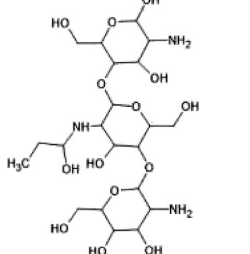
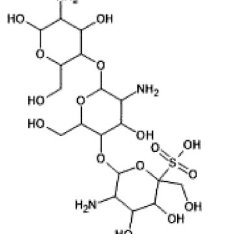
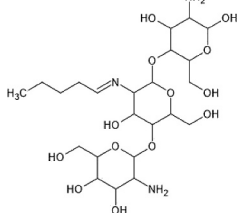
A blind docking on the overall protein structure to understand the putative sites for binding of the ligands and screening it for further target docking at the ACE2-RBD binding site.

Ligands	Binding affinity	Molecular weight	IUPAC name	Structure	Structure minimize energy (kcal/mol)
N-(2-chloro-6-fluorobenzyl)chitosan	-6.8	644.0409 Da	3-Amino-5-[(5-{[3-amino-4,5-dihydroxy-6-(hydroxymethyl)oxan-2-yl]oxy}-3-[(2-chloro-6-fluorophenyl)methyl]amino)-4-hydroxy-6-(hydroxymethyl)oxan-2-yl]oxy]-6-(hydroxymethyl)oxane-2,4-diol		E=664.02
N-benzoyl-O-acetylchitosan	-6.8	647.6255 Da	3-Amino-5-[(5-{[3-amino-4,5-dihydroxy-6-(hydroxymethyl)oxan-2-yl]oxy}-3-benzamido-4-hydroxy-6-(hydroxymethyl)oxan-2-yl]oxy]-2-hydroxy-6-(hydroxymethyl)oxan-4-yl acetate		E=647.04
N-(2-carboxyethyl)chitosan	-6.4	573.5455 Da	3-[(5-{[3-Amino-4,5-dihydroxy-6-(hydroxymethyl)oxan-2-yl]oxy}-2-{[5-amino-4,6-dihydroxy-2-(hydroxymethyl)oxan-3-yl]oxy}-4-hydroxy-6-(hydroxymethyl)oxan-3-yl]amino]propanoic acid		E=618.95
N-sulfo-chitosan	-6.4	581.546 Da	N-(5-{[3-amino-4,5-dihydroxy-6-(hydroxymethyl)oxan-2-yl]oxy}-2-{[5-amino-4,6-dihydroxy-2-(hydroxymethyl)oxan-3-yl]oxy}-4-hydroxy-6-(hydroxymethyl)oxan-3-yl)sulfamic acid		E=1079.65
Carboxymethyl chitosan	-6.3	543.5195 Da	N-(5-{[3-amino-4,5-dihydroxy-6-(hydroxymethyl)oxan-2-yl]oxy}-2-{[5-amino-4,6-dihydroxy-2-(hydroxymethyl)oxan-3-yl]oxy}-4-hydroxy-6-(hydroxymethyl)oxan-3-yl)acetamide		E=573.26
Chitosan oligosaccharide	-6.3	501.4828 Da	5-Amino-6-[(5-amino-6-{[5-amino-4,6-dihydroxy-2-(hydroxymethyl)oxan-3-yl]oxy}-4-hydroxy-2-(hydroxymethyl)oxan-3-yl]oxy]-2-(hydroxymethyl)oxane-3,4-diol		E=568.89
Dimethylpropyl amino-chitosan	-6.3	586.6303 Da	2,5-Diamino-6-[(5-amino-6-{[5-amino-4,6-dihydroxy-2-(hydroxymethyl)oxan-3-yl]oxy}-4-hydroxy-2-(hydroxymethyl)oxan-3-yl]oxy]-2-(hydroxymethyl)-4,5-dimethyl-3-propylhexane-3,4-diol		E=809.82

(continued on next page)

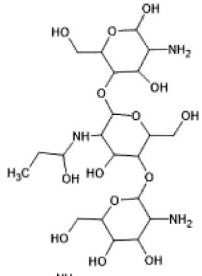
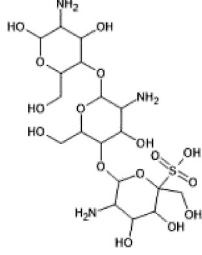
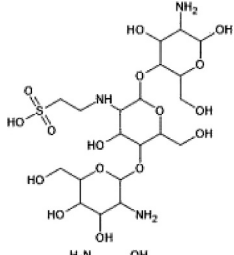
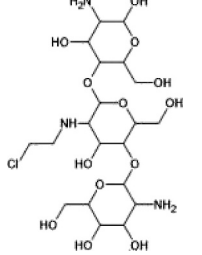
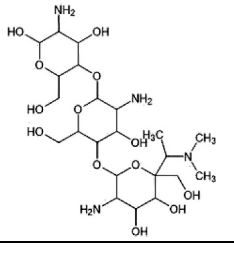


Table 6 (continued)

Ligands	Binding affinity	Molecular weight	IUPAC name	Structure	Structure minimize energy (kcal/mol)
N-sulfosuccinyl chitosan	-6.3	663.6035 Da	1-(5-([3-Amino-4,5-dihydroxy-6-(hydroxymethyl)oxan-2-yl]oxy)-2-([5-amino-4,6-dihydroxy-2-(hydroxymethyl)oxan-3-yl]oxy)-4-hydroxy-6-(hydroxymethyl)oxan-3-yl)-2,5-oxopyrrolidine-3-sulfonic acid		E=1187.73
Chitosan-chloride	-6.2	535.9279 Da	5-Amino-6-[(5-amino-6-([5-amino-4,6-dihydroxy-2-(hydroxymethyl)oxan-3-yl]oxy)-4-hydroxy-2-(hydroxymethyl)oxane-3,4-diol		E=600.24
Imino-chitosan	-6.2	514.4816 Da	5-Amino-6-[(6-([5-amino-4,6-dihydroxy-2-(hydroxymethyl)oxan-3-yl]oxy)-5-diazenyl-4-hydroxy-2-(hydroxymethyl)oxan-3-yl]oxy]-2-(hydroxymethyl)oxane-3,4-diol		E=554.21
O-sulfochitosan	-6.2	581.546 Da	{3-Amino-5-[(3-amino-5-([3-amino-4,5-dihydroxy-6-(hydroxymethyl)oxan-2-yl]oxy)-4-hydroxy-6-(hydroxymethyl)oxan-2-yl]oxy)-2-hydroxy-6-(hydroxymethyl)oxan-4-yl]oxidane sulfonic acid		E=1050.44
N-(3-chloro-2-hydroxypropyl) chitosan	-6.1	594.007 Da	5-Amino-6-[(6-([5-amino-4,6-dihydroxy-2-(hydroxymethyl)oxan-3-yl]oxy)-5-[(3-chloro-2-hydroxypropyl)amino]-4-hydroxy-2-(hydroxymethyl)oxan-3-yl]oxy)-2-(hydroxymethyl)oxane-3,4-diol		E=632.12
N-pentylidene-chitosan	-6	569.5998 Da	3-Amino-5-[(5-([3-amino-4,5-dihydroxy-6-(hydroxymethyl)oxan-2-yl]oxy)-4-hydroxy-6-(hydroxymethyl)-3-(pentylideneamino)oxan-2-yl]oxy]-6-(hydroxymethyl)oxane-2,4-diol		E=557.84

(continued on next page)

Table 6 (continued)

Ligands	Binding affinity	Molecular weight	IUPAC name	Structure	Structure minimize energy (kcal/mol)
N-(hydroxypropyl) chitosan	-5.9	559.5619 Da	3-Amino-5-[(5-[[3-amino-4,5-dihydroxy-6-(hydroxymethyl)oxan-2-yl]oxy]-4-hydroxy-6-(hydroxymethyl)-3-[[1-(hydroxypropyl)amino]oxan-2-yl]oxy]-6-(hydroxymethyl)oxane-2,4-diol		E=629.22
Sulfochitosan	-5.9	581.546 Da	5-Amino-6-[(5-amino-6-[[5-amino-4,6-dihydroxy-2-(hydroxymethyl)oxan-3-yl]oxy]-4-hydroxy-2-(hydroxymethyl)oxan-3-yl]oxy]-3,4-dihydroxy-2-(hydroxymethyl)oxane-2-sulfonic acid		E=1060.36
N-(2-sulfoethyl)chitosan	-5.8	609.5992 Da	2-[[5-[[3-Amino-4,5-dihydroxy-6-(hydroxymethyl)oxan-2-yl]oxy]-2-[[5-amino-4,6-dihydroxy-2-(hydroxymethyl)oxan-3-yl]oxy]-4-hydroxy-6-(hydroxymethyl)oxan-3-yl]amino]ethane-1-sulfonic acid		E=1051.96
N-(2-chloroethyl) chitosan	-5.6	563.981 Da	3-Amino-5-[(5-[[3-amino-4,5-dihydroxy-6-(hydroxymethyl)oxan-2-yl]oxy]-3-[[2-chloroethyl]amino]-4-hydroxy-6-(hydroxymethyl)oxan-2-yl]oxy]-6-(hydroxymethyl)oxane-2,4-diol		E=603.54
Dimethylaminoethyl-chitosan	-5.5	572.6038 Da	5-Amino-6-[(5-amino-6-[[5-amino-4,6-dihydroxy-2-(hydroxymethyl)oxan-3-yl]oxy]-4-hydroxy-2-(hydroxymethyl)oxan-3-yl]oxy]-2-[1-(dimethylamino)ethyl]-2-(hydroxymethyl)oxane-3,4-diol		E=817.32

### 3.2. ACE2 binding residues of RBD of SARS-CoV-2 as the target site

A library of Chitosan and Chitosan derivatives reported as antimicrobial and/or antiviral agents submitted in PubChem, Chem spider databases were screened for their binding affinity for the Receptor Binding Domain (RBD) of SARS-CoV-2 in complex with ACE2 receptor (PDB ID: 6M0J). They were blindly docked for understanding the putative binding affinity to RBD. There were promising results for the same as listed in Table 6. Out of the following derivatives, halogen derivatives and molecules with higher torsions (>20) and binding affinity lower than -6.0 kcal/mol were ruled out for further active target site docking. Halogen derivatives were ruled out because the bond formation by halogens with large protein system has not been understood at an atomic level, although a recent study by Milewska et al., based on the antiviral

efficacy of N-(2-hydroxypropyl)-3-trimethylammonium chitosan chloride (HTCC) against beta coronaviruses MERS-CoV of the same lineage to that to SARS-CoV-2 conducted in-vitro in Vero and Vero E6 cell lines and ex vivo studies conducted by deploying human airway epithelium (HAE) model reflected the potential of HTCC in hampering virus replication with a more pronounced effect on SARS-CoV-2 and MERS-CoV although they have a different viral entry mechanism. It also significantly inhibited the internalization of viruses into vulnerable cells by reacting with spike protein through electrostatic interactions but still, the exact mechanism is not widely understood [9,40]. On further docking at the putative active target sites loop at 484-509 residues, there was a significant reduction in binding affinity of screened residues, so again ligands with a binding affinity lower than -6.0 kcal/mol were ruled out. Among them, novel antimicrobial derivatives of chitosan N-

**Table 7**

List of hydrogen bonds and other bonds at protein-ligand interfaces targeting ACE2 binding residues of RBD.

Chemical bonds	SARS-CoV-2RBD-N-benzyl-O-acetyl chitosan (-6.6 kcal/mol)		SARS-CoV-2RBD-imino-chitosan (-6.0 kcal/mol)		SARS-CoV-2RBD-SCOS (-6.1 kcal/mol)		SARS-CoV-2RBD-ACE2	
	Residues	Length (Å)	Residues	Length (Å)	Residues	Length (Å)	Residues	Length (Å)
Hydrogen bonds	TYR449 (HH)	1.92	GLY496 (HN)	2.35	ARG403 (HH11)	2.48	ASN487 (ND2)	2.6
	TYR453 (HH)	2.00	THR500 (OG1)	2.47	ARG403 (HH11)	2.64	LYS417 (NZ)	3.0
	ASN501 (OD1)	2.34	ASN501 (OD1)	2.86	ARG403 (HH12)	2.72	GLN493 (NE2)	2.8
	THR500 (OG1)	2.12	ARG403 (CD)	3.22	GLY496 (HN)	2.23	TYR505 (OH)	3.2
	THR500 (O)	2.97	ASN501 (CA)	3.42	GLN498 (HE22)	2.85	TYR449 (OH)	2.7
	GLY496 (O)	3.50	ASN501 (OD1)	3.32	THR500 (HG1)	2.48	THR500 (OG1)	2.6
	SER494 (O)	3.53			GLY502 (HN)	1.85	ASN501 (N)	3.7
					THR500 (O)	2.40	TYR449 (OH)	3.0
					ARG403 (CD)	2.97	TYR489 (OH)	3.5
					GLN498 (OE1)	3.35	ASN487 (OD1)	2.7
							GLY 502 (N)	2.8
Other bonds	TYR505 ( $\pi$ - $\pi$ )	3.86			PHE497 ( $\pi$ -anion) <sup>a</sup>	4.87	LYS417 (NZ) <sup>a</sup>	3.9
					TYR505 ( $\pi$ -anion) <sup>a</sup>	3.71	LYS417 (NZ) <sup>a</sup>	3.0
					TYR449 ( $\pi$ -sulfur)	5.30		
					TYR495 ( $\pi$ -sulfur)	5.65		
					TYR505 ( $\pi$ -sulfur)	5.16		
					TYR505 ( $\pi$ -sulfur)	4.32		

<sup>a</sup> Salt bridge, HH: hydrogen eta, OD1: oxygen delta 1, OG1: oxygen gamma 1, O: oxygen, HN: nitrogen eta, NZ: nitrogen zeta, CD: carbon delta, CA: carbon alpha, HH11: hydrogen eta 11, HH12: hydrogen eta 12, HE22:hydrogen epsilon 22, HG1: hydrogen gamma 1, OE1: oxygen epsilon 1, ND2: nitrogen delta 2, NE2: nitrogen epsilon 2, OH: oxygen eta, N: nitrogen.

benzoyl-O-acetyl-chitosan (Pubchem CID 129851122), Imino-chitosan (Pubchem CID: 129887062), and antiviral Sulfated-chitosan oligosaccharide [17] had the best putative binding affinity. Later these ligands were further analyzed for multiple target sites. In Table 7, the breakup of all the hydrogen bonds types and other types of interaction formed by the selected moiety has been determined and analysis for each Ligand and conformation model is shown in both mesh surface and electrostatic surface (Fig. 7a-c). Also, these ligands were docked with the new variants P.1 (PDB ID: 7NXC) and B.1.1.7 (PDB ID: 7NEG). Interestingly, all three ligands could form putative strong hydrogen bonds with residue Asn 501 of RBD (wild type) than ACE2. The highest putative binding affinity of N-benzoyl-O-acetyl-chitosan (-6.3 kcal/mol), Imino-chitosan (-6.1 kcal/mol), and Sulfated-chitosan oligosaccharide (SCOS) (-6.1 kcal/mol) had to RBD of P.1 strain. The highest putative binding affinity of N-benzoyl-O-acetyl-chitosan (-6.3 kcal/mol), Imino-chitosan (-5.4 kcal/mol), and SCOS (-6.2 kcal/mol) had to RBD of B.1.1.7 strain. For both P.1 and B.1.1.7 lineages, ligands N-benzoyl-O-acetyl-chitosan and SCOS have shown putative strong hydrogen bonding on the mutated residue Tyr 501, which indicates to be associated in favour of SARS-CoV-2 spike glycoprotein in evading mAbs. Furthermore, previously only ligand N-benzoyl-O-acetyl-chitosan could form a putative strong hydrogen bond with residue Tyr 449 for wild type Table 7. This feature is retained irrespective of the mutation of three critical residues N501Y, E484K, K417T, and either of the combination, but it is to be noted the putative bond type varied with the combination of the type of mutation as putative strong hydrogen bond is seen in the case of N501Y mutated UK variant B.1.1.7. Moreover, there is disproportionate favourability for residue Tyr 449 for the other two ligands Imino-chitosan and SCOS. Since mutation at N501Y and E484K observed for P.1 lineage, has favoured Imino-chitosan to form a putative strong hydrogen bond with Tyr 449 (Fig. 8a-c), whereas for SCOS, the only mutation at N501Y seen B.1.1.7 has been favorable. Similarly, only ligand SCOS formed a putative strong hydrogen bond with Gln 498 for wild type, but mutation at Asn 501 has aided N-benzoyl-O-acetyl-chitosan to form a putative strong hydrogen bond with Gln 498 (Figs. 9a-b, 10). However, this interaction

is only valid for mutation at residue N501Y seen in UK variant B.1.1.7. The other major highlights are: 1) There was the absence of residue bonding to residue Gln 493 for all three ligands nonetheless mutation at residue N501Y elicited a putative hydrogen bond for N-benzoyl-O-acetyl-chitosan in both variants and SCOS in B.1.1.7 variant. 2) Mutation of K417T besides N501Y and E484K seen in P.1 variant has advocated putative hydrogen bondwithThr417 residues for ligands Imino-chitosan and SCOS. 3) Only the mutation at residue N501Y seen in B.1.1.7 has oddly accentuated strong salt bridge formation for ligand SCOS. Overall, it is to be noted that Imino-chitosan loses binding affinity to RBD of B.1.1.7 with a mutation at residue N501Y but this was countered in the case of P.1 variant with all the three mutations N501Y, E484K, and K417T. Moreover, these molecules were docked at lower molecular weight, than their proposed activity range (>3 kDa). On increasing their chain size and restricting the least significant rotatable bonds, higher binding affinity to RBD of S-protein for both wild type and new distinct variants has been noted.

### 3.3. Heparin binding site as a putative target site of RBD of SARS-CoV-2

Heparan sulfate proteoglycans (HSPGs) are receptors present in the cell surface's extracellular matrix, having a copolymeric composition of N-Acetyl-D-glucosamine D-glucuronic acid, which is responsible for the transport of a plethora of macromolecules [41,42]. However, these assemblies vary in length, size, and expression of cell types impacting their role as primary target receptors for endocytosis [43] of viral particles and tissue tropism characteristics through non-specific binding to viruses and their host cell for infection activation [44–46]. An abnormal coagulopathy was first reported by Tang et.al in where they conducted a study on 201 patients among which 84 developed Acute respiratory distress syndrome (ARDS) with higher prothrombin time (PT) in case of SARS-CoV-2 infected patients [47]. Later multiple studies reported the association between disease severity caused by SARS-CoV-2 and pulmonary embolism. Nonetheless, a study published by Clausenet.al., demonstrated that the HSPG receptors were a necessary cofactor for

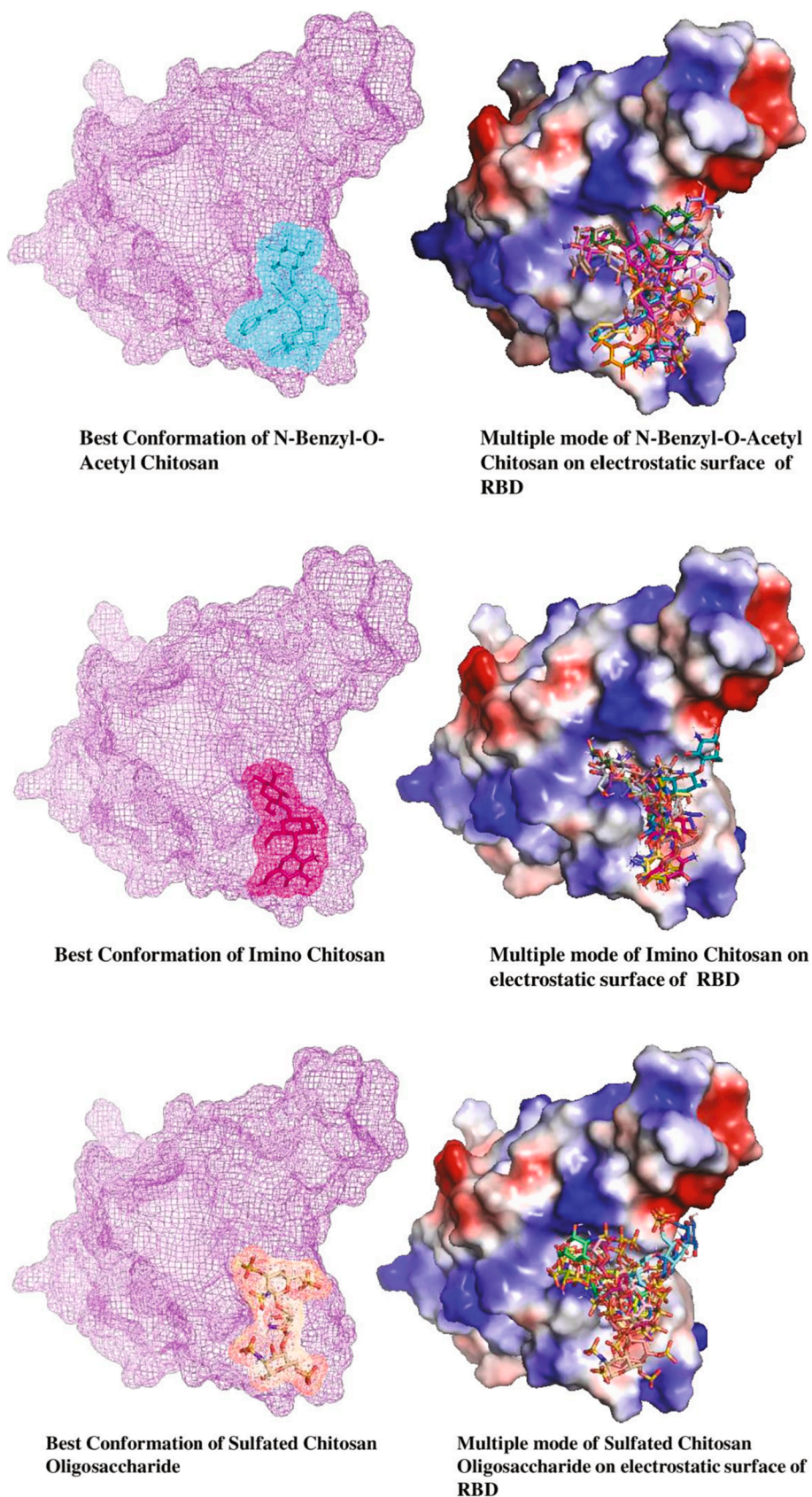


**Fig. 7.** a):Conformation models for N-benzyl-O-acetyl-chitosan in both mesh surface and electrostatic surface. b):Conformation models for Imino-chitosan in both mesh surface and electrostatic surface c):Conformation models for sulfated-chitosan oligosaccharide in both mesh surface and electrostatic surface.

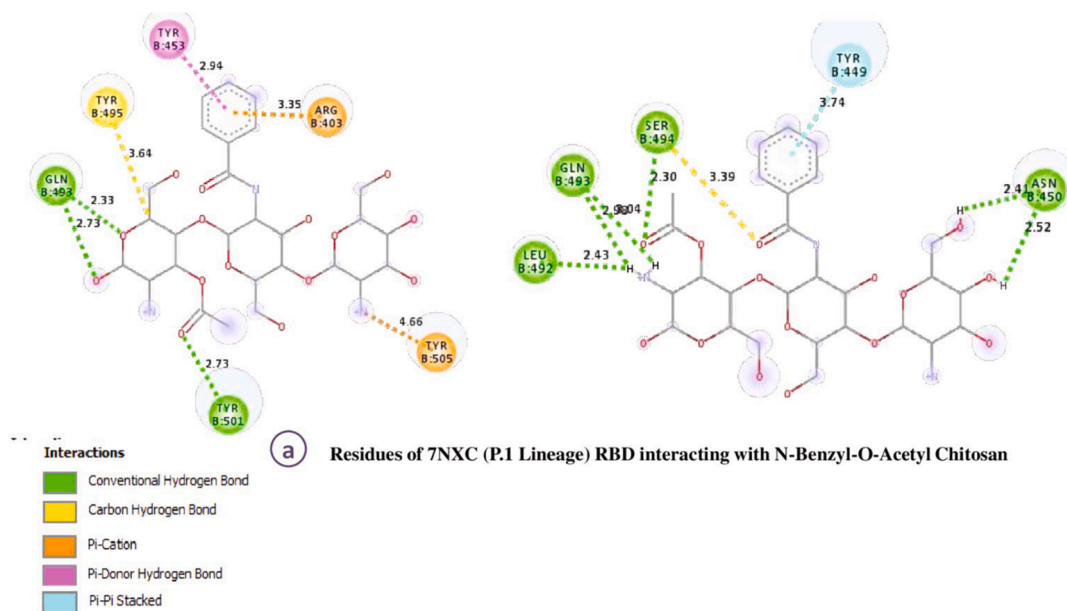


**Fig. 8.** a-c) Interaction of all three ligands with new variant P.1 Lineage RBD of SARS-CoV-2.

SARS-CoV-2 infection since it contributed to shifting the trimeric conformation of Spike glycoprotein from the closed state to open state conformation (RBM) by exposing the RBD of SARS-CoV-2 for efficient binding to ACE2 (Fig. 11). It observed the occupancy of the homotrimer by ACE2 increased from bearing 5% to 37% for one ACE2 and 21% for two ACE2 for pseudotype virus [14]. This explains the rationale behind the thrombosis in severely infected patients and virulence promoted by HSPGs. So, the use of the non-anticoagulant heparinoids and low molecular weight heparin for treatments protocol has been in the realm. Also, there are studies providing evidence of non-anticoagulant heparinoids and low molecular weight heparin engaged in blocking SARS-CoV-2 infection [14,48,49,50]. So we analyzed the ligands binding affinity to the suggested putative residues Arg 346, Phe 347, Ala 348, Ser349, Ala 352, Trp 353, Asn 354, Arg 355, Lys 356, Arg 357, Lys 444, Asn 448, Asn 450, Tyr 451, Arg 466, Arg 509 of RBD in a closed conformation state [14] as the active target site with heparin as +ve control. The fluctuation graph of both wild type (Fig. 5) and P.1 (Fig. 6) variant shows that the loop 346-358 and 440-457 has significantly low fluctuation which is similar to the critical loop of 484-509 in exposed state RBD complexed with ACE2. In Table 8, the breakup of all the hydrogen bonds types and other types of interaction formed by the selected moiety has been determined and analysis for each Ligand and conformation models are shown in (Fig. 12a-d). Intriguingly, the heparinoid-like property of SCOS is seen to be well reserved similar to the interaction between heparin disaccharide I—S and RBD. As there is the overlap of residues interaction common between heparin disaccharide I—S and sulfated-chitosan oligosaccharide and the types of bonds formed. Also, that low molecular SCOS has been reported to possess antiviral properties against HIV-1 [17] and the use of low molecular weight heparin as prophylactic treatment for severely infected has aided in reduced mortality from coagulopathy [51,52]. However, heparin's use comes with safety concerns in association with toxicity. So, lower toxicity analogues with antiviral properties such as SCOS have the potential therapeutic advantage in this regard. Moreover, it was observed that sulfation at the amino and 6-hydroxyl groups had superior activity than the 3-hydroxyl group, which was also reported by Clausen et al. [14]. This characteristic is well reserved in the case of SCOS. Moreover, the other two ligands N-benzoyl-O-acetyl-chitosan and Imino-chitosan also have significant putative binding affinity to the corresponding residues in the loop of interest. Also, it can be arguably concluded that

the backbone of N-acetyl glucosamine had a significant contribution to the binding affinity of RBD to chitosan derivatives along with the substrate chain for both in the case of heparinoid and non-heparinoids besides the added advantage to have similar effects on variants. Although there has been mutation at N501Y, E484K, and K417T for P.1 variant and N501Y for B.1.1.7 yet there was no notable geometric or orientation change in RBD with respect to the wild type which doesn't impede the putative binding affinity of the proposed ligands.

#### 3.4. Boceprevir binding to Main protease residues as a putative target site

Main protease ( $M^{pro}$ ) is a three-domain cysteine protease also known as 3C-Like protease domain ( $3CL^{pro}$ ) with a chymotrypsin-like two domain folds at N terminus present all CoVs. They protease mediates the maturation of CoVs by involving in most of the maturation process that occurs in cleavage events within the precursor polyprotein pp1a and pp1ab [53,54]. So they are essential along with Papain-like protease for the extensive proteolytic processing that liberates the functional polypeptides from the polyproteins. The  $M^{pro}$  ( $3CL^{pro}$ ) cleaves the polyprotein at 11 conserved sites involving Leu-Gln (Ser, Ala, Gly) sequences in HCoV-229E [55]. It cleaves two overlapping polyproteins [pp1a (replicase 1a, ~450 kD) and pp1ab (replicase 1ab, ~750 kD) to functional proteins, which is an essential step in viral replication was observed in 33.1 kDa HCoV-229E key proteinase activity [56]. Later a study report by Zhang et al., suggested that there was a 96% sequence identity between SARS-CoV and SARS-CoV-2 and that the  $M^{pro}$  was involved 11 cleavage sites on the larger polyproteins pp1ab Leu-Gln (Ser, Ala, Gly) making it an attractive antiviral drug target for SARS-CoV-2 [57,58]. So to elucidate the potential antiviral against  $M^{pro}$  by the three ligands of interest N-benzoyl-O-acetyl-chitosan, Imino-chitosan, and antiviral SCOS we did molecular docking at the putative binding site of Boceprevir. They demonstrated Boceprevir, and GC376, both efficaciously inhibit SARS-CoV-2 with  $EC_{50}$  of 15.57  $\mu$ M and 0.70  $\mu$ M in Vero cells by targeting the Main protease. To elucidate the mechanism, it was observed that Boceprevir had a putative hydrogen bond formation at the catalytically active site of SARS-CoV-2 Main protease as the main mechanism of inhibition space between the residues His41, Met49, Tyr54, Asn142-Cys145, His164-Glu166. Although GC376 had a potent inhibition than Boceprevir but had limitations in clinical perspective [21]. Detrimental side effects are seen in animal

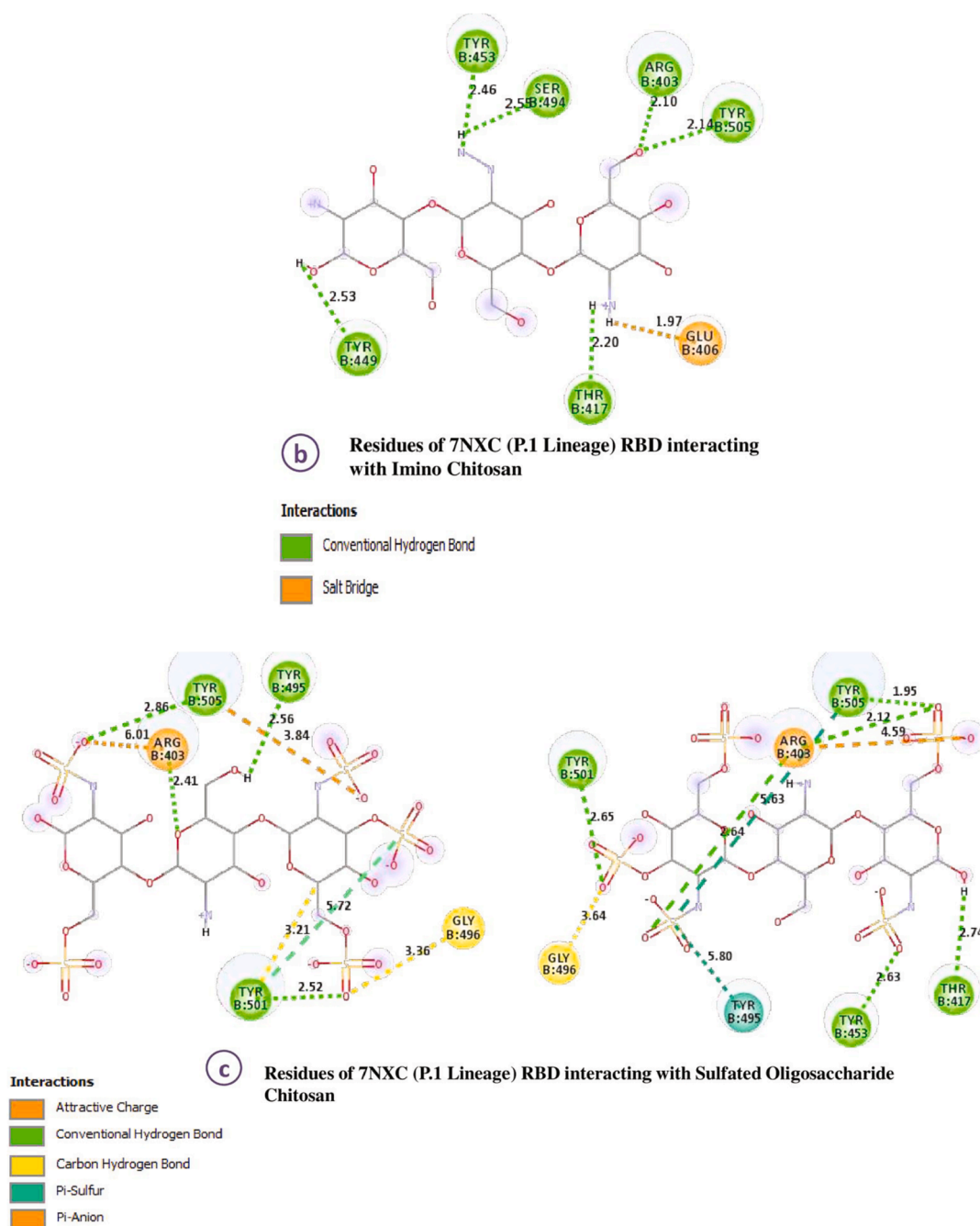


Fig. 8. (continued).

teeth in prospective with longer than 2 or more weeks [59,60]. Table 9 and Fig. 13 summarized the putative bonds formed by Borceprevir. In perspective to the ligands of interest, Imino-chitosan and N-benzyl-O-acetyl-chitosan had a high binding affinity at the catalytically active site of main proteases (Table 9 and Fig. 14a-b). However, the most notable ligand Imino-chitosan has a similar strong binding affinity towards the residue Glu166 that of Boceprevir.

### 3.5. Bioactivity prediction

Few physicochemical properties of the proposed ligands were predicted by bioactivity parameters, indicating their potential as a putative drug. The bioactivity of potential test ligands was calculated based on their chemical structure as reported in Table 10. The miscreen engine analyses a training collection of active structures and compares it to

inactive molecules using sophisticated Bayesian statistics in the Molinspiration method. For preparation, only SMILES or SDfile structures of active molecules are needed; no knowledge about the active site or binding is required.

### 3.6. ADME profile

The most significant pharmacokinetic properties of a drug are its absorption, distribution, metabolism, excretion, and toxicity profile, which include absorption, distribution, metabolism, excretion, and toxicity profile. The bioavailability of a drug is determined by its absorption. Bad compound solubility, chemical instability in the stomach, and failure to pass through the intestinal wall are all factors that can reduce the extent to which a drug is absorbed after its administration. The free/bound transfer of a drug from one compartment to another is

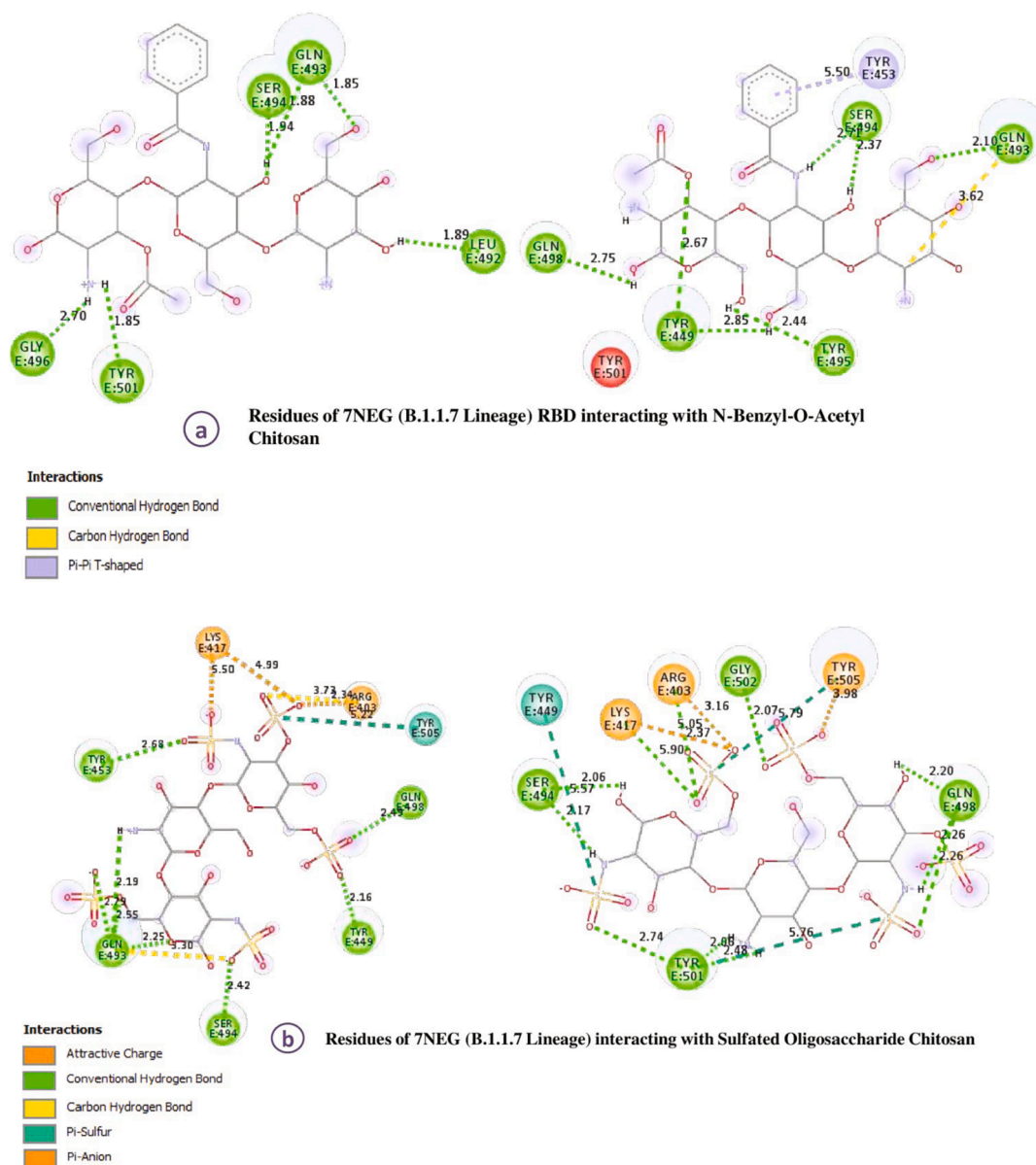


Fig. 9. a-b) Interaction of two of three ligands with new variant B.1.1.7 Lineage RBD of SARS-CoV-2.

known as drug delivery. Regional blood flow patterns, molecular size, polarity, and binding to serum proteins, which form a complex, are all factors that influence drug delivery. Drug metabolism occurs as a result of a variety of biological reactions that turn the drug into an inactive or more active form. This research is carried out to track the impact of a drug on particular metabolic pathways by measuring metabolite levels after it has been administered. This helps to build a full picture of a drug's impact on metabolism and pathways that are linked to the mechanism of treatment response variance. The excretion of metabolized drugs is just as significant as the other three aspects. ADME values of test ligands have been compiled in Table 11.

The drug's solubility score, or Log S, tells us about the drug's absorption properties in terms of Aqueous solubility. The drug's absorption property is connected to its passage through the GIT's walls and the drug's first pass impact. Being in the ideal range of solubility is the very first step. The drug's permeability through the blood-brain barrier (BBB) has a direct impact on absorption and delivery. The acceptable range of computational BBB for an ideal drug candidate is  $-3.0$  to  $1.2$ . All three ligands perfectly fit the necessity. The permeability of a drug in epithelial cells is determined by the  $\text{Ca-CO}_2$  value as it is a continuous

cell made up of heterogeneous human epithelial colorectal adenocarcinoma cells that are used to assess drug permeability across the cell's epithelial wall. Further ahead, the values of PPB% (Plasma Protein Binding) would analyze drug binding to plasma protein as a key distribution in the system. The higher the value, the more difficult it becomes for the drug to detach from the tightly bound protein and release in the system. P-gp, also known as P-glycoprotein, is a cell surface protein involved in xenobiotic efflux. Lastly, renal clearance is analyzed by MDCK-OCT (Madin Darby Canine Kidney-Organic Cation Transporter) which determines the post metabolism excretion of xenobiotics.

Drug ligand metabolism profiles were also simulated to see whether they interacted with the CYP450 enzyme family (Table 9). A family of microsomal enzymes known as cytochrome P450 is responsible for xenobiotic metabolism (CYP450). CYP3A4, CYP3A2, CYP2C9, CYP2C19, and CYP2D6 are all members of the CYP450 family, which are involved in the metabolism of various drugs. The ideal scenario of a drug should be the non-inhibition of these enzymes. Findings of the test ligands suggested that both Ligand 1 and ligand 2 be decent leads. However, the property of CYP450 inhibitory promiscuity refers to the capacity for a drug or chemical to bind to and decrease or diminish the

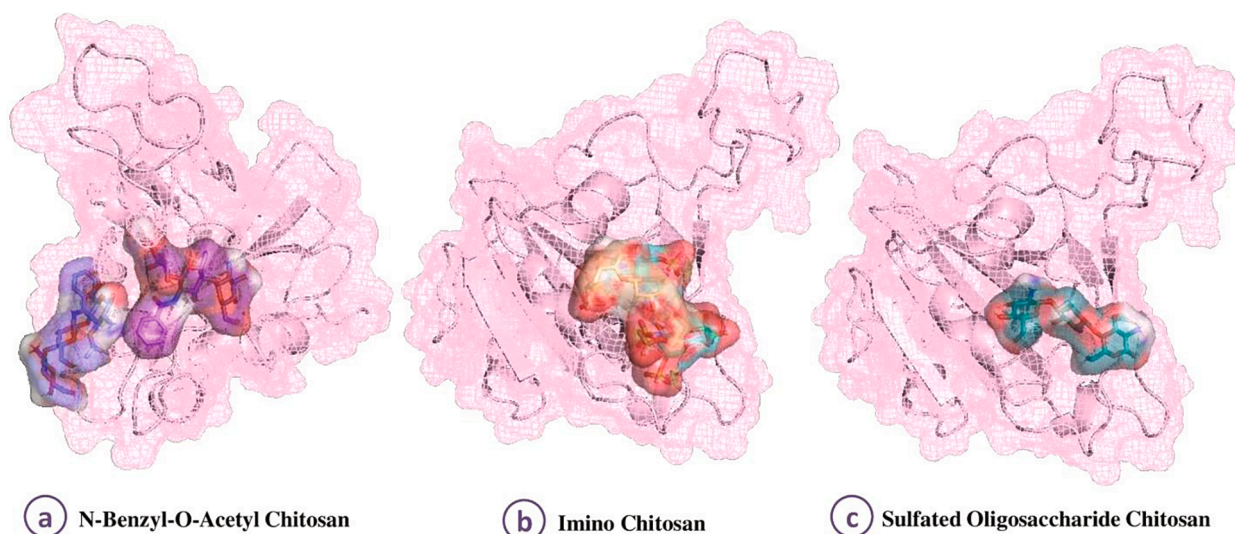


Fig. 10. Confirmation models of all three ligands against P.1 Lineage variant.

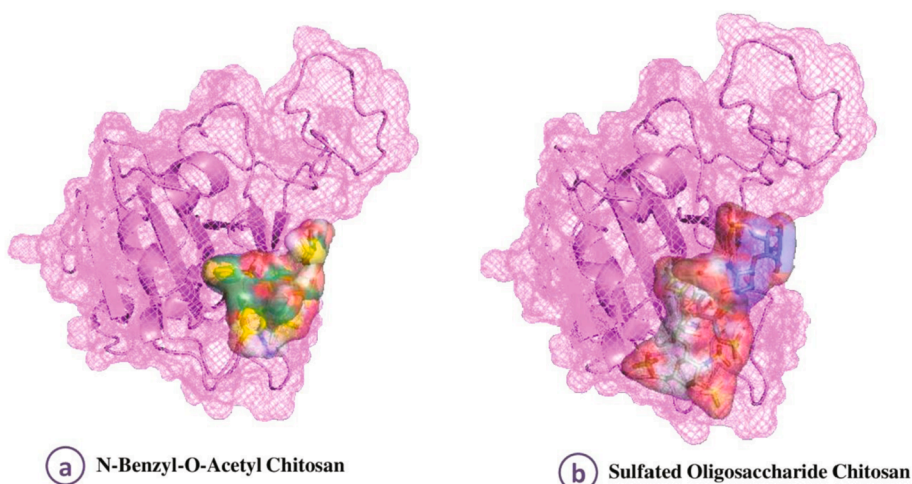


Fig. 11. Confirmation models of two of three ligands against B.1.1.7 Lineage variant.

activity of multiple different CYP450 isoform enzymes and it suggests that the chances of sulfated-chitosan oligosaccharide have proved to be relatively inefficient in this aspect whereas Imino-chitosan has divulged as the fittest candidate.

### 3.7. Toxicity analysis

Drug ligand metabolism profiles were also simulated to estimate their interactions with the CYP450 enzyme family Table 12. A family of microsomal enzymes known as cytochrome P450 (CYP450) is responsible for xenobiotic metabolism. CYP3A4, CYP3A2, CYP2C9, CYP2C19, and CYP2D6 are all members of the CYP450 family, which are involved in metabolizing various drugs. The ideal scenario of a drug should be the non-inhibition of these enzymes. In this regard, findings of the test ligands suggested both Ligand 1 and ligand 2 be the decent leads. The property of CYP450 inhibitory promiscuity refers to the capacity for a drug or chemical to bind to and decrease or diminish the activity of

multiple different CYP450 isoform enzymes suggests that the chances of sulfated-chitosan oligosaccharide have proved to be relatively inefficient in this aspect.

### 3.8. Toxicity analysis

The toxicity profile of drug ligands was determined on the basis of their mutagenic and carcinogenic properties, using the *in silico* Ames test, carcinogenicity test in rats and mice, and HERG inhibition results. All the results of the toxicity profile were favorable indicating that the ligands can be potential drugs Table 13. AMES test is used to predict whether the drug ligand is mutagenic or not. The mutagenicity, although is an important parameter but more sensitive aspect is carcinogenicity, whether a drug can cause cancer to the administered organism or not. The *in-silico* results of drug ligands were negative, indicating their administration to be safe in terms of their risk.



**Table 8**

List of hydrogen bonds and other bonds at protein-ligand interfaces and comparative analysis with +ve control Heparin.

Bonds	SARS-CoV-2 prefusion state-N-benzyl-O-acetyl chitosan (-6.3 kcal/mol)		SARS-CoV-2 prefusion state-Imino-chitosan (-6.0 kcal/mol)		SARS-CoV-2 Prefusion state-SCOS (-6.4 kcal/mol)		SARS-CoV-2 prefusion state-Heparin disaccharide- I–S (+ve control) (-5.9 kcal/mol)	
	Residues	Length (Å)	Residues	Length (Å)	Residues	Length (Å)	Residues	Length (Å)
Hydrogen bonds	SER349 (HN)	1.94	ARG346 (HN)	2.19	ARG346 (HN)	2.04	LYS356 (HZ1)	2.72
	ASN450 (HD21)	2.59	ASN354 (HD22)	2.30	ALA348 (HN)	2.43	LYS356 (HZ3)	2.51
	ARG346 (O)	2.22	ASN354 (OD1)	2.72	SER349 (HG)	2.74	THR345 (HN)	2.40
	ARG346 (O)	1.97	PHE347 (O)	2.97	SER349 (HG)	2.51	THR345 (HG1)	2.09
	ASN450 (O)	2.72	PHE347 (O)	2.87	ASN354 (HD21)	2.64	ALA348 (HN)	2.91
	ASN450 (O)	2.51	ARG346 (O)	2.33	ASN354 (HD21)	2.48	SER399 (HG)	2.14
			GLU340 (O)	2.13	ASN450 (HD21)	2.19	PHE347 (CA)	3.60
					ASN450 (HD22)	2.78		
					ARG466 (HH22)	2.53		
					ARG346 (O)	2.63		
					THR345 (CB)	3.55		
					THR345 (CB)	3.42		
					ALA348 (CA)	3.21		
					ALA352 (O)	3.65		
Other bonds	VAL341 ( $\pi$ -alkyl)	5.01	TYR451 ( $\pi$ -cation)	4.80	ARG466 (HD22) <sup>a</sup>	2.31	PHE347 ( $\pi$ -anion)	4.85
	ALA344 ( $\pi$ -alkyl)	4.41			LYS356 (NZ) <sup>a</sup>	5.50	LYS356 (HZ1) <sup>a</sup>	2.72
					PHE347 ( $\pi$ -anion)	4.96	LYS356 (HZ3) <sup>a</sup>	2.51

<sup>a</sup> Salt bridge HH: hydrogen eta, OD1: oxygen delta 1, OG1: oxygen gamma 1, O: oxygen, HN: nitrogen eta, NZ: nitrogen zeta, CD: carbon delta, CA: carbon alpha, HH11: hydrogen eta 11, HH12: hydrogen eta 12, HE22: hydrogen epsilon 22, HG1: hydrogen gamma 1, OE1: oxygen epsilon 1, ND2: nitrogen delta 2, NE2: nitrogen epsilon 2, OH: oxygen eta, N: nitrogen, HD21: hydrogen delta 21, HH22: hydrogen eta 22, CB: carbon beta, HG: hydrogen gamma, HZ1: hydrogen zeta 1, HZ3: hydrogen zeta 3.

### 3.9. Cross-reactivity profile with other beta coronaviruses

Although SARS-CoV-2 belongs to the class of *Betacoronaviruses* of lineage *Sarbecovirus*, there is a significant difference in the choice of receptors for each of the viruses from subclass *Sarbecovirus*. In a study led by Bate et al., the monoclonal antibodies against the specific structural proteins of the SARS-CoV virus were studied and characterized against the similar targets of the SARS-CoV-2 virus. The striking structural similarity between Envelope, Membrane and Nucleocapsid proteins as 96%, 91%, and 91% respectively were reserved for both the viruses. However, binding affinity analysis of potent mAbs CR3022 against the full-length spike protein and its RBD region showed partial neutralization of the spike protein. Other antibodies tested failed to present comparable binding affinity and neutralization properties. This could be due to changes in the residues of spike protein between two viruses [61]. Another study shed light on the cross-reactive antibodies observed in the pre-pandemic healthy donors against the S1 antigen of SARS-CoV-2 virus. This shows how conserved protein residues across various “common cold” related coronaviruses have been significant in kindling the immune system against the novel COVID-19 virus [62]. Along similar lines, it was observed that antibodies from the serum of mildly affected and naive COVID-19 patients showed cross-reactivity to seasonal coronavirus, HCoV NL-63, relatively higher in the latter case [63]. Although HCoV NL63 belongs to alpha coronaviruses. It happens to have a similar choice of receptor i.e., is ACE2 for cellular entry mechanism [64]. Interpreting the milk samples for the antibodies against S1 and S2 subunits of spike protein in the COVID-19 positive mothers put forward insightful results. The COVID-19 infected mothers’ milk showed high levels of HCoV-OC43 reactive IgG antibodies. Moreover, observing high IgM levels reactive to SARS-CoV-2, S1 subunit, and S1 + S2 subunits of HCoV-OC43 and HCoV-229E in two unexposed mothers suggest the presence of cross-reactive antibodies against human coronaviruses which could be due to similarity in epitopes on S1 and S2 subunits that are recognized by human milk antibodies [65]. Other reports supporting cross-reactive immunity by another study where low antibody titers against HCoV-EMC were reported in SARS-CoV-2 infected patients. The bioinformatic analysis reflected overlapping regions in the spike protein for both viruses [66]. Through the development of a multi-CoV antibody panel test, it was noted that there exists a positive correlation between the SARS-CoV-2 immune response and high hCoV

responses which could be due to similar host-pathogen interactions and viral proteins mode of action. It was observed that people have pre-existing immunity to human  $\alpha$ - (NL63 and 229E) and  $\beta$ -hCoVs (OC43 and HKU1) strains irrespective of their COVID-19 infection status and the same gets augmented post-SARS-CoV-2 infection due to cross-reactivity to spike trimer [67]. Quantification of pre-pandemic antibody levels in human serum samples revealed the presence of antibodies against HCoV virus and the same got amplified post-COVID-19 infection. A decent percentage of these antibodies cross-reacted with SARS-CoV-2 spike and nucleocapsid proteins but were not found to be associated with protection against SARS-CoV-2 hospitalizations or infections [68]. All these studies emphasize the overlapping of structural protein residues in different coronaviruses strains to some extent. However, a more concrete investigation is required to conclude something in this context. Based on what has come to the attention till date, the top three performers of this study ensure some degree of reactivity to the proteins of other coronavirus strains and thus, vouching for wide utility as a therapeutic intervention for future pandemics by the coronavirus family.

## 4. Conclusions

The need for new antiviral agents to combat the rising number of infections is well embraced, and this necessitates the discovery of novel viral-specific targets. In this work, we discuss three potential derivatives of Chitosan which can be used for both treatment and prophylactic against COVID-19 infection. Although there is the emergence of variants like B.1.1.7 (UK), B.1.351 (South African), and P.1 (Brazil) which has caused recent upticks in the case of numbers due to higher binding affinity to ACE2 receptors, the primary cell entry point for SARS-CoV-2 virus. The molecular docking studies show promising results for further clinical use of these derivatives. Moreover, SARS-CoV-2 has been reported to employ Heparan sulfate glycoprotein receptors for viral entry which is similar to what is employed by HCoV NL63 strain. This enabled us to explore multiple target sites against the spike glycoprotein receptor binding domain of SARS-CoV-2 for the prospective derivatives of interest. Besides, these derivatives have shown promising ADMET profile, augmenting their chances to be developed as potential therapeutic interventions against SARS-CoV-2 infection.

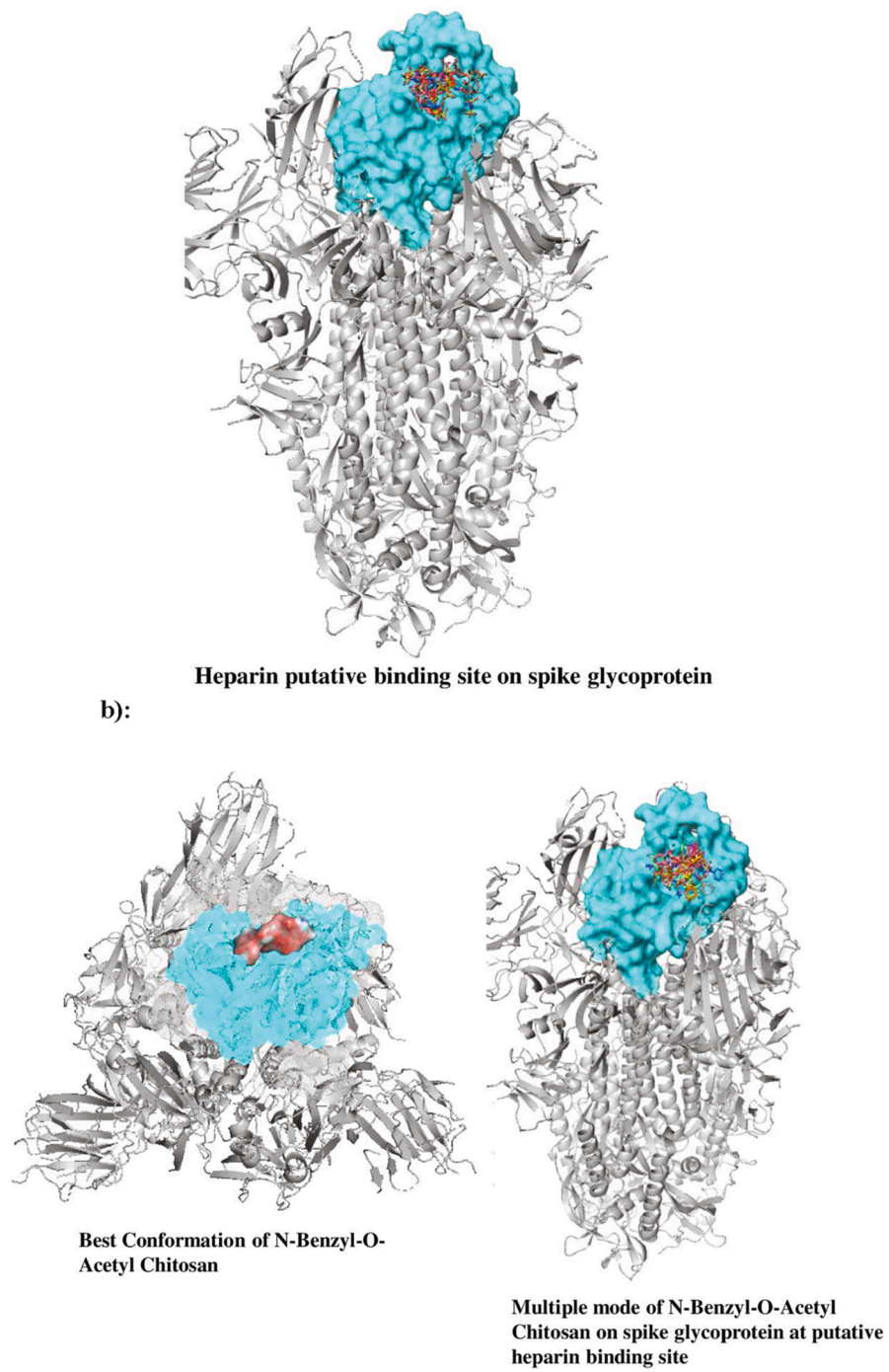


**Fig. 12.** a): Heparin models putative site. b): N-benzyl-O-acetyl-chitosan models at heparin putative sites. c): Imino-chitosan models at heparin putative sites. d): Sulfated-chitosan oligosaccharide models at heparin putative sites.

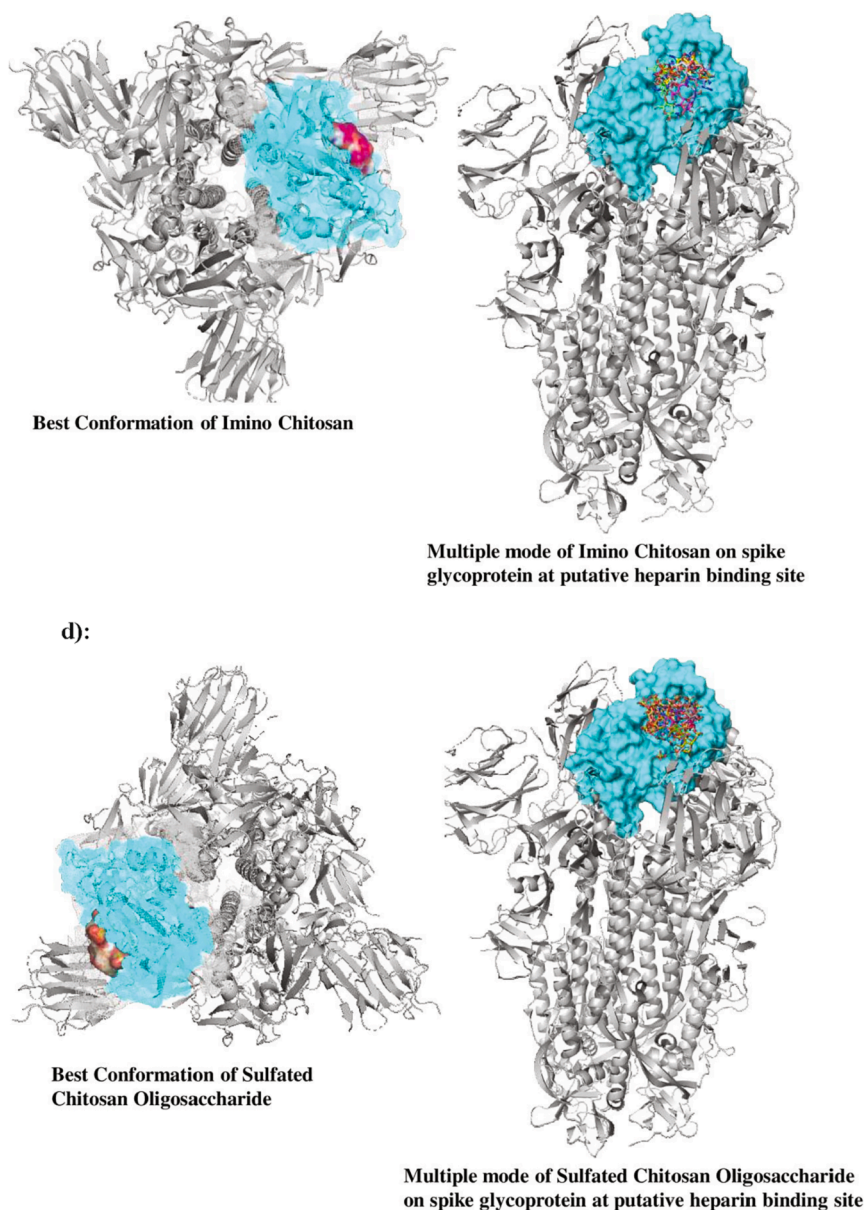


Fig. 12. (continued).

Table 9

List of hydrogen bonds and other bonds at Protein-Ligand interfaces and comparative analysis with +ve control Boceprevir.

Bonds	SARS-CoV-2 main protease-N-benzyl-O-acetyl-chitosan (-6.4 kcal/mol)		SARS-CoV-2 main protease-imino-chitosan (-6.7 kcal/mol)		SARS-CoV-2 main protease-Boceprevir + ve control (-6.7 kcal/mol)	
	Residues	Length (Å)	Residues	Length (Å)	Residues	Length (Å)
Hydrogen bonds	THR26 (HN)	1.99	LEU141 (O)	2.40	GLY143 (HN)	2.24
	THR24 (O)	2.11	GLU166 (O)	2.90	GLY143 (HN)	2.29
	THR26 (O)	2.52	GLU166 (OE1)	2.59	CYS145 (HN)	2.38
	THR26 (O)	2.33	GLU166 (O)	3.04	GLU166 (O)	2.38
Other bonds			HIS41 (ND1)	2.63		
			HIS41 (CE1)	3.60		
			GLU166 (OE1)	3.53		
	GLU166 ( $\pi$ -anion) <sup>a</sup>	3.32				

<sup>a</sup> Salt bridge, O: oxygen, HN: nitrogen eta, CE1: carbon epsilon 1, HE22:hydrogen epsilon 22, HE22:hydrogen epsilon 21, OE1: oxygen epsilon 1, ND1: nitrogen delta 1, † electrostatic.

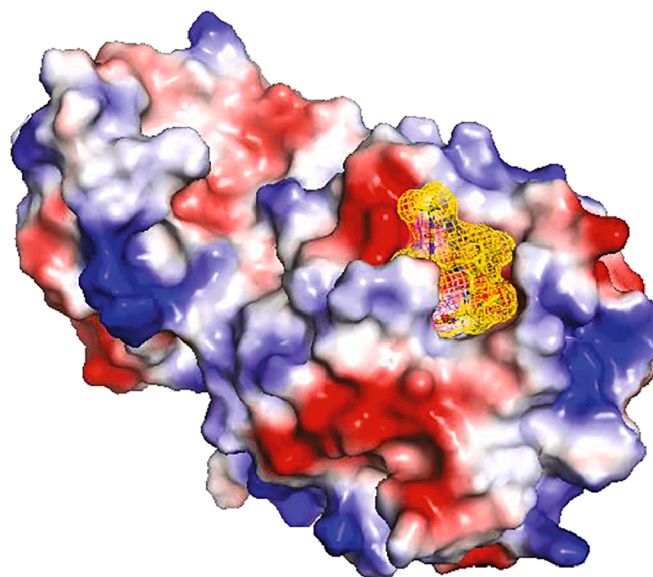


Fig. 13. Binding of boceprevir at the active site of the main protease at the catalytic active site.

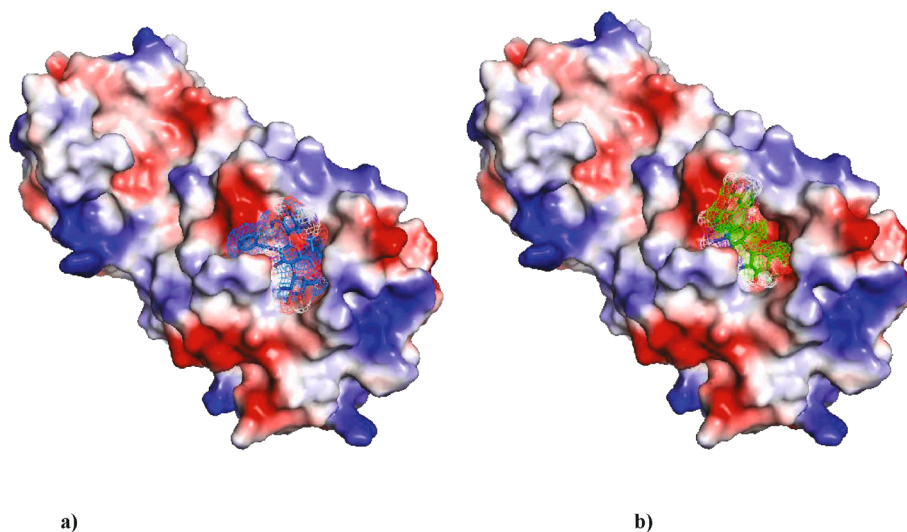


Fig. 14. a-b): Binding of ligands of interest at the active site of the main protease catalytic site.

**Table 10**  
Bioactivity prediction by physicochemical property analysis of test ligands.

Molecular descriptors	Imino-chitosan	N-benzyl-O-acetyl-chitosan	Sulfated-chitosan oligosaccharide
LogP	-1.4	-6.35	-3.73
TPSA	296.26	511.08	286.06
Volume	432.71	614.52	425.86
MW	514.49	896.77	501.49
n-atoms	35	54	34
Acceptor HB	17	31	16
Donor HB	13	9	14
n-rotb	8	7	17

**Table 11**  
Comparative analysis of absorption, distribution, and excretion profiling of test ligands.

Properties	Acceptable range	Imino-chitosan	N-benzyl-O-acetyl-chitosan	Sulfated-chitosan oligosaccharide
Human oral absorption%	80-100	80	89	72
Log S	-6.5/0.5	-1.0047	-1.4243	-0.8103
Blood-brain barrier	- 3.0 to 1.2	0.9550	0.9526	0.9257
Human intestinal absorption	70-100	0.8609	0.9367	0.6649
Caco-2 permeability	25 - 500	74.30	82.72	78.74
PPB%	25/100	74.70	81.19	94.90
Pgp-inhibition	Non-inhibitor	Non-inhibitor	Non-inhibitor	Inhibitor
Renal organic cation transporter	25-500	429.2	250.7	46.3

**Table 12**  
Predictive CYP family-based drug metabolism profile of test ligands.

Properties	Imino-chitosan	N-benzyl-o-acetyl-chitosan	Sulfated-chitosan oligosaccharide
CYP450 2C9 substrate	Non-substrate	Non-substrate	Non-substrate
CYP450 2D6 substrate	Non-substrate	Non-substrate	Non-substrate
CYP450 3A4 substrate	Non-substrate	Non-substrate	Non-substrate
CYP450 1A2 inhibitor	Non-inhibitor	Non-inhibitor	Inhibitor
CYP450 2C9 inhibitor	Non-inhibitor	Non-inhibitor	Inhibitor
CYP450 2D6 inhibitor	Non-inhibitor	Non-inhibitor	Non-inhibitor
CYP450 2C19 inhibitor	Non-inhibitor	Non-inhibitor	Inhibitor
CYP450 3A4 inhibitor	Non-inhibitor	Non-inhibitor	Non-inhibitor
CYP inhibitory promiscuity	Low CYP inhibitory promiscuity	Low CYP inhibitory promiscuity	Low CYP inhibitory promiscuity

**Table 13**  
Toxicity prediction and analysis of test ligands.

Properties	Imino-chitosan	N-benzyl-o-acetyl-chitosan	Sulfated-chitosan oligosaccharide
Human ether-a-go-go-related gene inhibition	Weak inhibitor Non-inhibitor	Weak inhibitor Non-inhibitor	Weak inhibitor Non-inhibitor
AMES toxicity Carcinogens	Non AMES toxic Non-carcinogens	Non AMES toxic Non-carcinogens	Non AMES toxic Non-carcinogens
Biodegradation	Not ready biodegradable	Not ready biodegradable	Not ready biodegradable
Acute oral toxicity	III	III	IV
Rat acute toxicity	1.9354	2.4521	1.4577

**CRedit authorship contribution statement****Chandrima Modak:** Investigation, Methodology, Draft preparation.**Anubhuti Jha:** Investigation, Methodology, Draft preparation.**Nivya Sharma:** Methodology, Draft preparation.**Awanish Kumar:** Conceptualization, Methodology, Reviewing, Editing, and Finalizing draft.**Declaration of competing interest**

The authors have no conflict of interest to declare.

**Acknowledgments**

The authors are grateful to the National Institute of Technology (NIT) Raipur, BITS Pilani, and NIPER Hyderabad, India for providing all kinds of support to this work.

**References**

- U. Poudel, D. Subedi, S. Pantha, S. Dhakal, Animal coronaviruses and coronavirus disease 2019: lesson for one health approach, *Open Vet. J.* 10 (2020) 239–251.
- M.-Y. Wang, R. Zhao, L.-J. Gao, X.-F. Gao, D.-P. Wang, J.-M. Cao, SARS-CoV-2: structure, biology, and structure-based therapeutics development, *Front. Cell. Infect. Microbiol.* 10 (2020).
- P. Wang, M.S. Nair, L. Liu, S. Iketani, Y. Luo, Y. Guo, M. Wang, J. Yu, B. Zhang, P. D. Kwong, B.S. Graham, J.R. Mascola, J.Y. Chang, M.T. Yin, M. Sobieszczyk, C. A. Kyratsous, L. Shapiro, Z. Sheng, Y. Huang, D.D. Ho, Antibody resistance of SARS-CoV-2 variants B.1.351 and B.1.1.7, *BioRxiv*. (2021), <https://doi.org/10.1101/2021.01.25.428137>.
- A. Awadasseid, Y. Wu, Y. Tanaka, W. Zhang, Current advances in the development of SARS-CoV-2 vaccines, *Int. J. Biol. Sci.* 17 (2021) 8.
- N. Sharma, C. Modak, P.K. Singh, R. Kumar, D. Khatri, S.B. Singh, Underscoring the immense potential of chitosan in fighting a wide spectrum of viruses: a plausible molecule against SARS-CoV-2? *Int. J. Biol. Macromol.* 179 (2021) 33–44.
- M.R. Kumar, R. Muzzarelli, C. Muzzarelli, H. Sashiwa, A.J. Domb, Chitosan chemistry and pharmaceutical perspectives, *Chem. Rev.* 104 (2004) 6017–6084.
- M. Kong, X.G. Chen, K. Xing, H.J. Park, Antimicrobial properties of chitosan and mode of action: a state of the art review, *Int. J. Food Microbiol.* 144 (2010) 51–63.
- S.N. Chirkov, The antiviral activity of chitosan (review), *Prikl. Biokhim. Mikrobiol.* 38 (2002) 5–13.
- A. Milewska, K. Kaminski, J. Ciejka, K. Kosowicz, S. Zeglen, J. Wojarski, M. Nowakowska, K. Szczubialka, K. Pyrc, HTCC, Broad range inhibitor of coronavirus entry, *PLoS One* 11 (2016), e0156552.
- P. V'kovski, A. Kratzel, S. Steiner, H. Stalder, V. Thiel, Coronavirus biology and replication: implications for SARS-CoV-2, *Nat. Rev. Microbiol.* (2020) 1–16.
- J. Lan, J. Ge, J. Yu, S. Shan, H. Zhou, S. Fan, Q. Zhang, X. Shi, Q. Wang, L. Zhang, Structure of the SARS-CoV-2 spike receptor-binding domain bound to the ACE2 receptor, *Nature* 581 (2020) 215–220.
- J. Shang, G. Ye, K. Shi, Y. Wan, C. Luo, H. Aihara, Q. Geng, A. Auerbach, F. Li, Structural basis of receptor recognition by SARS-CoV-2, *Nature* 581 (2020) 221–224.
- S. Wang, F. Guo, K. Liu, H. Wang, S. Rao, P. Yang, C. Jiang, Endocytosis of the receptor-binding domain of SARS-CoV spike protein together with virus receptor ACE2, *Virus Res.* 136 (2008) 8–15.
- T.M. Clausen, D.R. Sandoval, C.B. Spliid, J. Pihl, H.R. Perrett, C.D. Painter, A. Narayanan, S.A. Majowicz, E.M. Kwong, R.N. McVicar, SARS-CoV-2 infection depends on cellular heparan sulfate and ACE2, *Cell* 183 (2020) 1043–1057.
- J. Cai, Q. Dang, C. Liu, B. Fan, J. Yan, Y. Xu, J. Li, Preparation and characterization of N-benzoyl-O-acetyl-chitosan, *Int. J. Biol. Macromol.* 77 (2015) 52–58.
- L. Marin, D. Ailincai, M. Mares, E. Paslaru, M. Cristea, V. Nica, B.C. Simionescu, Imino-chitosan biopolymeric films obtaining, self-assembling, surface and antimicrobial properties, *Carbohydr. Polym.* 117 (2015) 762–770.
- M. Artan, F. Karadeniz, M.Z. Karagozlu, M.-M. Kim, S.-K. Kim, Anti-HIV-1 activity of low molecular weight sulfated chitooligosaccharides, *Carbohydr. Res.* 345 (2010) 656–662.
- M. McCallum, A.C. Walls, J.E. Bowen, D. Corti, D. Velesler, Structure-guided covalent stabilization of coronavirus spike glycoprotein trimers in the closed conformation, *Nat. Struct. Mol. Biol.* 27 (2020) 942–949.
- P. Supasa, D. Zhou, W. Dejnirattisai, C. Liu, A.J. Mentzer, H.M. Ginn, Y. Zhao, H. M. Duyvesteyn, R. Nutalai, A. Tuekprakhon, Reduced neutralization of SARS-CoV-2 B. 1.1. 7 variant by convalescent and vaccine sera, *Cell* 184 (8) (2021) 2201–2211.e7.
- W. Dejnirattisai, D. Zhou, P. Supasa, C. Liu, A.J. Mentzer, H.M. Ginn, Y. Zhao, H. M. Duyvesteyn, A. Tuekprakhon, R. Nutalai, Antibody evasion by the P. 1 strain of SARS-CoV-2, *Cell* 184 (11) (2021) 2939–2954.e9.
- L. Fu, F. Ye, Y. Feng, F. Yu, Q. Wang, Y. Wu, C. Zhao, H. Sun, B. Huang, P. Niu, Both boceprevir and GC376 efficaciously inhibit SARS-CoV-2 by targeting its main protease, *Nat. Commun.* 11 (2020) 1–8.
- R.A. Laskowski, M.W. MacArthur, D.S. Moss, J.M. Thornton, PROCHECK: a program to check the stereochemical quality of protein structures, *J. Appl. Crystallogr.* 26 (1993) 283–291.
- J. Wang, W. Wang, P.A. Kollman, D.A. Case, Automatic atom type and bond type perception in molecular mechanical calculations, *J. Mol. Graph. Model.* 25 (2006) 247–260.
- A. Vangone, R. Spinelli, V. Scarano, L. Cavallo, R. Oliva, COCOMAPS: a web application to analyze and visualize contacts at the interface of biomolecular complexes, *Bioinformatics* 27 (2011) 2915–2916.
- S.J. Hubbard, J.M. Thornton, naccess, *Comput. Program Dep. Biochem. Mol. Biol. Univ. Coll. Lond.* 2 (1993).
- I.K. McDonald, J.M. Thornton, Satisfying hydrogen bonding potential in proteins, *J. Mol. Biol.* 238 (1994) 777–793.
- A. Kuriata, A.M. Gierut, T. Oleniecki, M.P. Ciemny, A. Kolinski, M. Kurcinski, S. Kmiecik, CABS-flex 2.0: a web server for fast simulations of flexibility of protein structures, *Nucleic Acids Res.* 46 (2018) W338–W343.
- M. Kurcinski, T. Oleniecki, M.P. Ciemny, A. Kuriata, A. Kolinski, S. Kmiecik, CABS-flex standalone: a simulation environment for fast modeling of protein flexibility, *Bioinformatics* 35 (2019) 694–695.
- M. Letko, A. Marzi, V. Munster, Functional assessment of cell entry and receptor usage for SARS-CoV-2 and other lineage B betacoronaviruses, *Nat. Microbiol.* 5 (2020) 562–569.
- A.C. Walls, Y.-J. Park, M.A. Tortorici, A. Wall, A.T. McGuire, D. Velesler, Structure, function, and antigenicity of the SARS-CoV-2 spike glycoprotein, *Cell* 181 (2020) 281–292.e6, <https://doi.org/10.1016/j.cell.2020.02.058>.
- M. Yuan, N.C. Wu, X. Zhu, C.-C.D. Lee, R.T. So, H. Lv, C.K. Mok, I.A. Wilson, A highly conserved cryptic epitope in the receptor binding domains of SARS-CoV-2 and SARS-CoV, *Science* 368 (2020) 630–633.
- K. Wu, G. Peng, M. Wilken, R.J. Geraghty, F. Li, Mechanisms of host receptor adaptation by severe acute respiratory syndrome coronavirus, *J. Biol. Chem.* 287 (2012) 8904–8911.
- F. Li, W. Li, M. Farzan, S.C. Harrison, Structure of SARS coronavirus spike receptor-binding domain complexed with receptor, *Science* 309 (2005) 1864–1868.
- A. Ali, R. Vijayan, Dynamics of the ACE2–SARS-CoV-2/SARS-CoV spike protein interface reveal unique mechanisms, *Sci. Rep.* 10 (2020) 1–12.
- R. Yan, Y. Zhang, Y. Li, L. Xia, Y. Guo, Q. Zhou, Structural basis for the recognition of SARS-CoV-2 by full-length human ACE2, *Science* 367 (2020) 1444–1448.
- M. Chand, Investigation of novel SARS-COV-2 variant: variant of concern 202012/01 (PDF), *Public Health Engl. PHE* (2020) 1–17.

- [37] K. Leung, M.H. Shum, G.M. Leung, T.T. Lam, J.T. Wu, Early transmissibility assessment of the N501Y mutant strains of SARS-CoV-2 in the United Kingdom, October to November 2020, *Eurosurveillance*. 26 (2021) 2002106.
- [38] CDC, Coronavirus disease 2019 (COVID-19), *Cent. Dis. Control Prev.* (2020). <https://www.cdc.gov/coronavirus/2019-ncov/science/science-briefs/scientific-brief-e-merging-variants.html>.
- [39] Y. Weisblum, F. Schmidt, F. Zhang, J. DaSilva, D. Poston, J.C. Lorenzi, F. Muecksch, M. Rutkowska, H.-H. Hoffmann, E. Michailidis, Escape from neutralizing antibodies by SARS-CoV-2 spike protein variants, *elife* 9 (2020), e61312.
- [40] A. Milewska, Y. Chi, A. Szczepanski, E. Barreto-Duran, K. Liu, D. Liu, X. Guo, Y. Ge, J. Li, L. Cui, HTCC as a highly effective polymeric inhibitor of SARS-CoV-2 and MERS-CoV, *BioRxiv*. (2020). Preprint.
- [41] M. Belting, Heparan sulfate proteoglycan as a plasma membrane carrier, *Trends Biochem. Sci.* 28 (2003) 145–151.
- [42] S. Sarrazin, W.C. Lamanna, J.D. Esko, Heparan sulfate proteoglycans, *Cold Spring Harb. Perspect. Biol.* 3 (2011), a004952.
- [43] H.C. Christianson, M. Belting, Heparan sulfate proteoglycan as a cell-surface endocytosis receptor, *Matrix Biol.* 35 (2014) 51–55.
- [44] A. Milewska, M. Zarebski, P. Nowak, K. Stozek, J. Potempa, K. Pyrc, Human coronavirus NL63 utilizes heparan sulfate proteoglycans for attachment to target cells, *J. Virol.* 88 (2014) 13221–13230.
- [45] J. Lang, N. Yang, J. Deng, K. Liu, P. Yang, G. Zhang, C. Jiang, Inhibition of SARS pseudovirus cell entry by lactoferrin binding to heparan sulfate proteoglycans, *PLoS One*. 6 (2011), e23710.
- [46] D. WuDUNN, P.G. Spear, Initial interaction of herpes simplex virus with cells is binding to heparan sulfate, *J. Virol.* 63 (1989) 52–58.
- [47] N. Tang, D. Li, X. Wang, Z. Sun, Abnormal coagulation parameters are associated with poor prognosis in patients with novel coronavirus pneumonia, *J. Thromb. Haemost.* 18 (2020) 844–847.
- [48] L. Liu, P. Chopra, X. Li, M.A. Wolfert, S.M. Tompkins, G.-J. Boons, SARS-CoV-2 spike protein binds heparan sulfate in a length-and sequence-dependent manner, *BioRxiv*. 16 (2020) 23.
- [49] C.J. Mycroft-West, D. Su, S. Elli, Y. Li, S.E. Guimond, G.J. Miller, J.E. Turnbull, E. A. Yates, M. Guerrini, D.G. Fernig, The 2019 coronavirus (SARS-CoV-2) surface protein (Spike) S1 receptor binding domain undergoes conformational change upon heparin binding, *BioRxiv*. 18 (2020) 48.
- [50] R. Tandon, J.S. Sharp, F. Zhang, V.H. Pomin, N.M. Ashpole, D. Mitra, M. G. McCandless, W. Jin, H. Liu, P. Sharma, Effective inhibition of SARS-CoV-2 entry by heparin and enoxaparin derivatives, *J. Virol.* 95 (2021).
- [51] N. Tang, H. Bai, X. Chen, J. Gong, D. Li, Z. Sun, Anticoagulant treatment is associated with decreased mortality in severe coronavirus disease 2019 patients with coagulopathy, *J. Thromb. Haemost.* 18 (2020) 1094–1099.
- [52] M. Levi, J. Thachil, T. Iba, J.H. Levy, Coagulation abnormalities and thrombosis in patients with COVID-19, *Lancet Haematol.* 7 (2020), e438.
- [53] A.E. Gorbalenya, E.V. Koonin, A.P. Donchenko, V.M. Blinov, Coronavirus genome: prediction of putative functional domains in the non-structural polyprotein by comparative amino acid sequence analysis, *Nucleic Acids Res.* 17 (1989) 4847–4861.
- [54] J. Ziebuhr, E.J. Snijder, A.E. Gorbalenya, Virus-encoded proteinases and proteolytic processing in the nidovirales, *Microbiology* 81 (2000) 853–879.
- [55] R. Hilgenfeld, From SARS to MERS: crystallographic studies on coronavirus proteases enable antiviral drug design, *FEBS J.* 281 (2014) 4085–4096.
- [56] J. Ziebuhr, J. Herold, S.G. Siddell, Characterization of a human coronavirus (strain 229E) 3C-like proteinase activity, *J. Virol.* 69 (1995) 4331–4338.
- [57] L. Zhang, D. Lin, X. Sun, U. Curth, C. Drosten, L. Sauerhering, S. Becker, K. Rox, R. Hilgenfeld, Crystal structure of SARS-CoV-2 main protease provides a basis for design of improved  $\alpha$ -ketoamide inhibitors, *Science* 368 (2020) 409–412.
- [58] X. Xue, H. Yu, H. Yang, F. Xue, Z. Wu, W. Shen, J. Li, Z. Zhou, Y. Ding, Q. Zhao, Structures of two coronavirus main proteases: implications for substrate binding and antiviral drug design, *J. Virol.* 82 (2008) 2515–2527.
- [59] N.C. Pedersen, Y. Kim, H. Liu, A.C. Galasiti Kankanamalage, C. Eckstrand, W. C. Groutas, M. Bannasch, J.M. Meadows, K.-O. Chang, Efficacy of a 3C-like protease inhibitor in treating various forms of acquired feline infectious peritonitis, *J. Feline Med. Surg.* 20 (2018) 378–392.
- [60] Y. Kim, H. Liu, A.C. Galasiti Kankanamalage, S. Weerasekara, D.H. Hua, W. C. Groutas, K.-O. Chang, N.C. Pedersen, Reversal of the progression of fatal coronavirus infection in cats by a broad-spectrum coronavirus protease inhibitor, *PLoS Pathog.* 12 (2016), e1005531.
- [61] T.A. Bates, J.B. Weinstein, H.C. Leier, W.B. Messer, F.G. Tafesse, Cross-reactivity of SARS-CoV structural protein antibodies against SARS-CoV-2, *Cell Rep.* 34 (2021), 108737.
- [62] M.C. Dalakas, K. Bitzogli, H. Alexopoulos, Anti-SARS-CoV-2 antibodies within IVIg preparations: cross-reactivities with seasonal coronaviruses, natural autoimmunity, and therapeutic implications, *Front. Immunol.* 12 (2021), 627285, <https://doi.org/10.3389/fimmu.2021.627285>.
- [63] L. Hens, T. Scholz, C. von Rhein, I. Wieters, F. Borgans, F.J. Eberhardt, K. Zacharowski, S. Ciesek, G. Rohde, M. Vehreschild, C. Stephan, T. Wolf, H. Hofmann-Winkler, H. Scheiblaue, B.S. Schnierle, Analysis of humoral immune responses in patients with severe acute respiratory syndrome coronavirus 2 infection, *J. Infect. Dis.* 223 (2021) 56–61, <https://doi.org/10.1093/infdis/jiaa680>.
- [64] H. Hofmann, K. Pyrc, L. Van Der Hoek, M. Geier, B. Berkhout, S. Pöhlmann, Human coronavirus NL63 employs the severe acute respiratory syndrome coronavirus receptor for cellular entry, *Proc. Natl. Acad. Sci.* 102 (2005) 7988–7993.
- [65] V. Demers-Mathieu, C. DaPra, G. Mathijssen, D.A. Sela, K.M. Jarvinen, A. Seppo, S. Fels, E. Medo, Human Milk antibodies against S1 and S2 subunits from SARS-CoV-2, HCoV-OC43, and HCoV-229E in mothers with a confirmed COVID-19 PCR, viral SYMPTOMS, and unexposed mothers, *Int. J. Mol. Sci.* 22 (2021), <https://doi.org/10.3390/ijms22041749>.
- [66] K.-H. Chan, J.F.-W. Chan, H. Tse, H. Chen, C.C.-Y. Lau, J.-P. Cai, A.K.-L. Tsang, X. Xiao, K.K.-W. To, S.K.-P. Lau, P.C.-Y. Woo, B.-J. Zheng, M. Wang, K.-Y. Yuen, Cross-reactive antibodies in convalescent SARS patients' sera against the emerging novel human coronavirus EMC (2012) by both immunofluorescent and neutralizing antibody tests, *J. Infect.* 67 (2013) 130–140, <https://doi.org/10.1016/j.jinf.2013.03.015>.
- [67] M. Becker, M. Strengert, D. Junker, P.D. Kaiser, T. Kerrinnes, B. Traenkle, H. Dinter, J. Häring, S. Ghozzi, A. Zeck, F. Weise, A. Peter, S. Hörber, S. Fink, F. Ruoff, A. Dulovic, T. Bakchoul, A. Baillot, S. Lohse, M. Cornberg, T. Illig, J. Gottlieb, S. Smola, A. Karch, K. Berger, H.-G. Rammensee, K. Schenke-Layland, A. Nelde, M. Märklin, J.S. Heitmann, J.S. Walz, M. Templin, T.O. Joos, U. Rothbauer, G. Krause, N. Schneiderhan-Marra, Exploring beyond clinical routine SARS-CoV-2 serology using MultiCoV-ab to evaluate endemic coronavirus cross-reactivity, *Nat. Commun.* 12 (2021) 1152, <https://doi.org/10.1038/s41467-021-20973-3>.
- [68] UPenn COVID Processing Unit, E.M. Anderson, E.C. Goodwin, A. Verma, C. P. Arevalo, M.J. Bolton, M.E. Weirick, S. Gouma, C.M. McAllister, S.R. Christensen, J. Weaver, P. Hicks, T.B. Manzoni, O. Oniyide, H. Ramage, D. Mathew, A.E. Baxter, D.A. Oldridge, A.R. Greenplate, J.E. Wu, C. Alanio, K. D'Andrea, O. Kuthuru, J. Dougherty, A. Pattekar, J. Kim, N. Han, S.A. Apostolidis, A.C. Huang, L.A. Vella, E.J. Wherry, N.J. Meyer, S. Cherry, P. Bates, D.J. Rader, S.E. Hensley, Seasonal human coronavirus antibodies are boosted upon SARS-CoV-2 infection but not associated with protection, *MedRxiv Prepr. Serv. Health Sci.* (2020), <https://doi.org/10.1101/2020.11.06.20227215>.